Fermi National Accelerator Laboratory

FERMILAB-Pub-98/327-E
CDF

Kinematics of $t\bar{t}$ Events at CDF

F. Abe et al.
The CDF Collaboration

Fermi National Accelerator Laboratory
P.O. Box 500, Batavia, Illinois 60510

November 1998

Submitted to *Physical Review D*

Operated by Universities Research Association Inc. under Contract No. DE-AC02-76CH03000 with the United States Department of Energy

CDF/PUB/TOP/CDFR/3985

Version 6.1

October 12, 1998

Kinematics of $t\bar{t}$ events at CDF

F. Abe,[17] H. Akimoto,[39] A. Akopian,[31] M. G. Albrow,[7] A. Amadon,[5] S. R. Amendolia,[27] D. Amidei,[20] J. Antos,[33] S. Aota,[37] G. Apollinari,[31] T. Arisawa,[39] T. Asakawa,[37] W. Ashmanskas,[5] M. Atac,[7] P. Azzi-Bacchetta,[25] N. Bacchetta,[25] S. Bagdasarov,[31] M. W. Bailey,[22] P. de Barbaro,[30] A. Barbaro-Galtieri,[18] V. E. Barnes,[29] B. A. Barnett,[15] M. Barone,[9] G. Bauer,[19] T. Baumann,[11] F. Bedeschi,[27] S. Behrends,[3] S. Belforte,[27] G. Bellettini,[27] J. Bellinger,[40] D. Benjamin,[35] J. Bensinger,[3] A. Beretvas,[7] J. P. Berge,[7] J. Berryhill,[5] S. Bertolucci,[9] S. Bettelli,[27] B. Bevensee,[26] A. Bhatti,[31] K. Biery,[7] C. Bigongiari,[27] M. Binkley,[7] D. Bisello,[25] R. E. Blair,[1] C. Blocker,[3] K. Bloom,[20] S. Blusk,[30] A. Bodek,[30] W. Bokhari,[26] G. Bolla,[29] Y. Bonushkin,[4] D. Bortoletto,[29] J. Boudreau,[28] L. Breccia,[2] C. Bromberg,[21] N. Bruner,[22] R. Brunetti,[2] E. Buckley-Geer,[7] H. S. Budd,[30] K. Burkett,[11] G. Busetto,[25] A. Byon-Wagner,[7] K. L. Byrum,[1] M. Campbell,[20] A. Caner,[27] W. Carithers,[18] D. Carlsmith,[40] J. Cassada,[30] A. Castro,[25] D. Cauz,[36] A. Cerri,[27] P. S. Chang,[33] P. T. Chang,[33] H. Y. Chao,[33] J. Chapman,[20] M. -T. Cheng,[33] M. Chertok,[34] G. Chiarelli,[27] C. N. Chiou,[33] F. Chlebana,[7] L. Christofek,[13] R. Cropp,[14] M. L. Chu,[33] S. Cihangir,[7] A. G. Clark,[10] M. Cobal,[27] E. Cocca,[27] M. Contreras,[5] J. Conway,[32] J. Cooper,[7] M. Cordelli,[9] D. Costanzo,[27] C. Couyoumtzelis,[10] D. Cronin-Hennessy,[6] R. Culbertson,[5] D. Dagenhart,[38] T. Daniels,[19] F. DeJongh,[7] S. Dell'Agnello,[9] M. Dell'Orso,[27] R. Demina,[7] L. Demortier,[31] M. Deninno,[2] P. F. Derwent,[7] T. Devlin,[32] J. R. Dittmann,[6] S. Donati,[27] J. Done,[34] T. Dorigo,[25] N. Eddy,[13] K. Einsweiler,[18] J. E. Elias,[7] R. Ely,[18] E. Engels, Jr.,[28] W. Erdmann,[7] D. Errede,[13] S. Errede,[13] Q. Fan,[30] R. G. Feild,[41] Z. Feng,[15] C. Ferretti,[27] I. Fiori,[2] B. Flaugher,[7] G. W. Foster,[7] M. Franklin,[11] J. Freeman,[7] J. Friedman,[19] H. Frisch,[5] Y. Fukui,[17] S. Gadomski,[14] S. Galeotti,[27] M. Gallinaro,[26] O. Ganel,[35] M. Garcia-Sciveres,[18] A. F. Garfinkel,[29] C. Gay,[41] S. Geer,[7] D. W. Gerdes,[20] P. Giannetti,[27] N. Giokaris,[31] P. Giromini,[9] G. Giusti,[27] M. Gold,[22] A. Gordon,[11] A. T. Goshaw,[6] Y. Gotra,[28] K. Goulianos,[31]

H. Grassmann,[36] C. Green,[29] L. Groer,[32] C. Grosso-Pilcher,[5] G. Guillian,[20] J. Guimaraes da Costa,[15] R. S. Guo,[33] C. Haber,[18] E. Hafen,[19] S. R. Hahn,[7] R. Hamilton,[11] T. Handa,[12] R. Handler,[40] W. Hao,[35] F. Happacher,[9] K. Hara,[37] A. D. Hardman,[29] R. M. Harris,[7] F. Hartmann,[16] J. Hauser,[4] E. Hayashi,[37] J. Heinrich,[26] A. Heiss,[16] B. Hinrichsen,[14] K. D. Hoffman,[29] C. Holck,[26] R. Hollebeek,[26] L. Holloway,[13] Z. Huang,[20] B. T. Huffman,[28] R. Hughes,[23] J. Huston,[21] J. Huth,[11] H. Ikeda,[37] M. Incagli,[27] J. Incandela,[7] G. Introzzi,[27] J. Iwai,[39] Y. Iwata,[12] E. James,[20] H. Jensen,[7] U. Joshi,[7] E. Kajfasz,[25] H. Kambara,[10] T. Kamon,[34] T. Kaneko,[37] K. Karr,[38] H. Kasha,[41] Y. Kato,[24] T. A. Keaffaber,[29] K. Kelley,[19] R. D. Kennedy,[7] R. Kephart,[7] D. Kestenbaum,[11] D. Khazins,[6] T. Kikuchi,[37] B. J. Kim,[27] H. S. Kim,[14] S. H. Kim,[37] Y. K. Kim,[18] L. Kirsch,[3] S. Klimenko,[8] D. Knoblauch,[16] P. Koehn,[23] A. Köngeter,[16] K. Kondo,[37] J. Konigsberg,[8] K. Kordas,[14] A. Korytov,[8] E. Kovacs,[1] W. Kowald,[6] J. Kroll,[26] M. Kruse,[30] S. E. Kuhlmann,[1] E. Kuns,[32] K. Kurino,[12] T. Kuwabara,[37] A. T. Laasanen,[29] S. Lami,[27] S. Lammel,[7] J. I. Lamoureux,[3] M. Lancaster,[18] M. Lanzoni,[27] G. Latino,[27] T. LeCompte,[1] S. Leone,[27] J. D. Lewis,[7] M. Lindgren,[4] T. M. Liss,[13] J. B. Liu,[30] Y. C. Liu,[33] N. Lockyer,[26] O. Long,[26] M. Loreti,[25] D. Lucchesi,[27] P. Lukens,[7] S. Lusin,[40] J. Lys,[18] K. Maeshima,[7] P. Maksimovic,[11] M. Mangano,[27] M. Mariotti,[25] J. P. Marriner,[7] G. Martignon,[25] A. Martin,[41] J. A. J. Matthews,[22] P. Mazzanti,[2] K. McFarland,[30] P. McIntyre,[34] P. Melese,[31] M. Menguzzato,[25] A. Menzione,[27] E. Meschi,[27] S. Metzler,[26] C. Miao,[20] T. Miao,[7] G. Michail,[11] R. Miller,[21] H. Minato,[37] S. Miscetti,[9] M. Mishina,[17] S. Miyashita,[37] N. Moggi,[27] E. Moore,[22] Y. Morita,[17] A. Mukherjee,[7] T. Muller,[16] A. Munar,[27] P. Murat,[27] S. Murgia,[21] M. Musy,[36] H. Nakada,[37] T. Nakaya,[5] I. Nakano,[12] C. Nelson,[7] D. Neuberger,[16] C. Newman-Holmes,[7] C.-Y. P. Ngan,[19] L. Nodulman,[1] A. Nomerotski,[8] S. H. Oh,[6] T. Ohmoto,[12] T. Ohsugi,[12] R. Oishi,[37] M. Okabe,[37] T. Okusawa,[24] J. Olsen,[40] C. Pagliarone,[27] R. Paoletti,[27] V. Papadimitriou,[35] S. P. Pappas,[41] N. Parashar,[27] A. Parri,[9] J. Patrick,[7] G. Pauletta,[36] M. Paulini,[18] A. Perazzo,[27] L. Pescara,[25] M. D. Peters,[18] T. J. Phillips,[6] G. Piacentino,[27] M. Pillai,[30] K. T. Pitts,[7] R. Plunkett,[7] A. Pompos,[29] L. Pondrom,[40] J. Proudfoot,[1] F. Ptohos,[11] G. Punzi,[27] K. Ragan,[14] D. Reher,[18] M. Reischl,[16] A. Ribon,[25] F. Rimondi,[2] L. Ristori,[27] W. J. Robertson,[6] A. Robinson,[14] T. Rodrigo,[27] S. Rolli,[38] L. Rosenson,[19] R. Roser,[13] T. Saab,[14] W. K. Sakumoto,[30] D. Saltzberg,[4] A. Sansoni,[9] L. Santi,[36] H. Sato,[37] P. Schlabach,[7]

E. E. Schmidt,[7] M. P. Schmidt,[41] A. Scott,[4] A. Scribano,[27] S. Segler,[7] S. Seidel,[22] Y. Seiya,[37] F. Semeria,[2] T. Shah,[19] M. D. Shapiro,[18] N. M. Shaw,[29] P. F. Shepard,[28] T. Shibayama,[37] M. Shimojima,[37] M. Shochet,[5] J. Siegrist,[18] A. Sill,[35] P. Sinervo,[14] P. Singh,[13] K. Sliwa,[38] C. Smith,[15] F. D. Snider,[15] J. Spalding,[7] T. Speer,[10] P. Sphicas,[19] F. Spinella,[27] M. Spiropulu,[11] L. Spiegel,[7] L. Stanco,[25] J. Steele,[40] A. Stefanini,[27] R. Ströhmer,[7a] J. Strologas,[13] F. Strumia, [10] D. Stuart,[7] K. Sumorok,[19] J. Suzuki,[37] T. Suzuki,[37] T. Takahashi,[24] T. Takano,[24] R. Takashima,[12] K. Takikawa,[37] M. Tanaka,[37] B. Tannenbaum,[4] F. Tartarelli,[27] W. Taylor,[14] M. Tecchio,[20] P. K. Teng,[33] Y. Teramoto,[24] K. Terashi,[37] S. Tether,[19] D. Theriot,[7] T. L. Thomas,[22] R. Thurman-Keup,[1] M. Timko,[38] P. Tipton,[30] A. Titov,[31] S. Tkaczyk,[7] D. Toback,[5] K. Tollefson,[30] A. Tollestrup,[7] H. Toyoda,[24] W. Trischuk,[14] J. F. de Troconiz,[11] S. Truitt,[20] J. Tseng,[19] N. Turini,[27] T. Uchida,[37] F. Ukegawa,[26] J. Valls,[32] S. C. van den Brink,[15] S. Vejcik, III,[20] G. Velev,[27] I. Volobouev,[18] R. Vidal,[7] R. Vilar,[7a] D. Vucinic,[19] R. G. Wagner,[1] R. L. Wagner,[7] J. Wahl,[5] N. B. Wallace,[27] A. M. Walsh,[32] C. Wang,[6] C. H. Wang,[33] M. J. Wang,[33] A. Warburton,[14] T. Watanabe,[37] T. Watts,[32] R. Webb,[34] C. Wei,[6] H. Wenzel,[16] W. C. Wester, III,[7] A. B. Wicklund,[1] E. Wicklund,[7] R. Wilkinson,[26] H. H. Williams,[26] P. Wilson,[7] B. L. Winer,[23] D. Winn,[20] D. Wolinski,[20] J. Wolinski,[21] S. Worm,[22] X. Wu,[10] J. Wyss,[27] A. Yagil,[7] W. Yao,[18] K. Yasuoka,[37] G. P. Yeh,[7] P. Yeh,[33] J. Yoh,[7] C. Yosef,[21] T. Yoshida,[24] I. Yu,[7] A. Zanetti,[36] F. Zetti,[27] and S. Zucchelli[2]

(CDF Collaboration)

[1] *Argonne National Laboratory, Argonne, Illinois 60439*

[2] *Istituto Nazionale di Fisica Nucleare, University of Bologna, I-40127 Bologna, Italy*

[3] *Brandeis University, Waltham, Massachusetts 02254*

[4] *University of California at Los Angeles, Los Angeles, California 90024*

[5] *University of Chicago, Chicago, Illinois 60637*

[6] *Duke University, Durham, North Carolina 27708*

[7] *Fermi National Accelerator Laboratory, Batavia, Illinois 60510*

[8] *University of Florida, Gainesville, Florida 32611*

[9] *Laboratori Nazionali di Frascati, Istituto Nazionale di Fisica Nucleare, I-00044 Frascati, Italy*

[10] *University of Geneva, CH-1211 Geneva 4, Switzerland*

[11] *Harvard University, Cambridge, Massachusetts 02138*

[12] *Hiroshima University, Higashi-Hiroshima 724, Japan*

[13] *University of Illinois, Urbana, Illinois 61801*

[14] *Institute of Particle Physics, McGill University, Montreal H3A 2T8, and University of Toronto, Toronto M5S 1A7, Canada*

[15] *The Johns Hopkins University, Baltimore, Maryland 21218*

[16] *Institut für Experimentelle Kernphysik, Universität Karlsruhe, 76128 Karlsruhe, Germany*

[17] *National Laboratory for High Energy Physics (KEK), Tsukuba, Ibaraki 305, Japan*

[18] *Ernest Orlando Lawrence Berkeley National Laboratory, Berkeley, California 94720*

[19] *Massachusetts Institute of Technology, Cambridge, Massachusetts 02139*

[20] *University of Michigan, Ann Arbor, Michigan 48109*

[21] *Michigan State University, East Lansing, Michigan 48824*

[22] *University of New Mexico, Albuquerque, New Mexico 87131*

[23] *The Ohio State University, Columbus, Ohio 43210*

[24] *Osaka City University, Osaka 588, Japan*

[25] *Universita di Padova, Istituto Nazionale di Fisica Nucleare, Sezione di Padova, I-35131 Padova, Italy*

[26] *University of Pennsylvania, Philadelphia, Pennsylvania 19104*

[27] *Istituto Nazionale di Fisica Nucleare, University and Scuola Normale Superiore of Pisa, I-56100 Pisa, Italy*

[28] *University of Pittsburgh, Pittsburgh, Pennsylvania 15260*

[29] *Purdue University, West Lafayette, Indiana 47907*

[30] *University of Rochester, Rochester, New York 14627*

[31] *Rockefeller University, New York, New York 10021*

[32] *Rutgers University, Piscataway, New Jersey 08855*

[33] *Academia Sinica, Taipei, Taiwan 11530, Republic of China*

[34] *Texas A&M University, College Station, Texas 77843*

[35] *Texas Tech University, Lubbock, Texas 79409*

[36] *Istituto Nazionale di Fisica Nucleare, University of Trieste/ Udine, Italy*

[37] *University of Tsukuba, Tsukuba, Ibaraki 305, Japan*

[38] *Tufts University, Medford, Massachusetts 02155*

[39] *Waseda University, Tokyo 169, Japan*

[40] *University of Wisconsin, Madison, Wisconsin 53706*

[41] *Yale University, New Haven, Connecticut 06520*

(CDF Collaboration)

The kinematic properties of $t\bar{t}$ events are studied in the W + multijet channel using data collected with the CDF detector during the 1992-1995 runs at the Tevatron Collider corresponding to an integrated luminosity of 109 pb^{-1}. Distributions of a variety of kinematic variables chosen to be sensitive to different aspects of $t\bar{t}$ production are compared with those expected from Monte Carlo calculations. A sample of 34 events rich in $t\bar{t}$ pairs is obtained by requiring at least one jet identified by the silicon vertex detector (SVX) as having a displaced vertex consistent with the decay of a b hadron. The data are found to be in good agreement with predictions of the leading order $t\bar{t}$ matrix element with color coherent parton shower evolution.

PACS numbers: 14.65.Ha, 13.85.Ni, 13.85.Qk

I. INTRODUCTION

The discovery of the top quark was reported in 1995 by both CDF [1] and D0 [2]. The technique used in Ref. [1] is an extension of the method presented in the first direct evidence for the top quark [3]. At a center of mass energy $\sqrt{s} = 1.8$ TeV top is predominantly produced in $t\bar{t}$ pairs which decay almost all of the time into $W^+ \, b \, W^- \, \bar{b}$. The most sensitive measure of $t\bar{t}$ production in the CDF detector was found to be the number of events with at least one jet tagged by the silicon vertex detector (SVX) [4] as a b-quark jet candidate (b-jet) in events which have one W that decays leptonically plus three or more jets [5]. The

b-jets are tagged by identifying displaced secondary vertices from the decay of long-lived b hadrons. Ref. [1] reported 27 SVX b-tagged jets compared to 6.7 ± 2.1 expected from background in the $W + \geq 3$ jet sample from 67 pb^{-1} of integrated luminosity. In addition to b-tagging, studies of specific kinematic variables in the $W + \geq 3$ jet events found strong evidence of $t\bar{t}$ production [6, 7]. Both tagging and kinematic techniques were useful in establishing the existence of $t\bar{t}$ production.

Having established the existence of the top quark, it is important to determine whether the production and decay mechanisms are correctly described by the standard model. Differences between predictions and the observed kinematic features could arise if higher order effects are important or if non-standard model contributions are present. Candidates for non-standard model production that would affect the purity of top events and thus the spectra of the final-state jets or leptons include resonant states that decay to $t\bar{t}$ [8] producing peaks in the $t\bar{t}$ invariant mass distribution or supersymmetric top squarks [9] that give rise to top-like final states. The validity of the standard model predictions for the production and decay of top are an important consideration for precision measurements of intrinsic properties such as the top quark mass [3, 10, 11]. In this paper, the standard model predictions are tested by comparing the calculations of kinematic properties using QCD Monte Carlo event generators with their measured counterparts in the data [12, 13]. The data was collected during the 1992-1995 runs representing a total integrated luminosity of 109 ± 7 pb^{-1}. The 34 $W + \geq 3$ jet events with at least one b-tagged jet [5] provide a data sample which has a large, well determined $t\bar{t}$ fraction with very little kinematic bias due to the tagging.

Sections II through V of the paper describe the data sets, review the available Monte Carlo generators for both standard model $t\bar{t}$ production and the QCD W+jets background, and define the selection of kinematic variables used to compare Monte Carlo predictions and data. In Section VI, the sensitivity of predictions for the kinematic properties of the $t\bar{t}$ events to the modeling of QCD radiation, the mass of the top quark, and detector effects is studied. Section VII compares the data to Monte Carlo predictions using the first moments of the kinematic distributions for a diverse selection of variables. Section VIII presents a more detailed comparison of kinematic distributions using both differential and integral plots including statistical tests of the comparisons. The conclusions are summarized in Section IX.

II. DATA SETS

The data sets were chosen to include events with $t\bar{t}$ pairs which decay into W^+ b W^- $\bar{b}$ with one W decaying into $e\nu$ or $\mu\nu$ and other W decaying into quarks [1]. The jets are reconstructed with a fixed cone algorithm [14] using a cone size R = $\sqrt{\Delta\eta^2 + \Delta\phi^2} = 0.4$ (where $\Delta\phi$ is the cone half-width in azimuth and $\Delta\eta$ is the cone half-width in pseudorapidity) [15]. The jets are ordered in observed transverse energy E_T = E sin(θ) where E is the scalar sum of the calorimeter energy inside the jet cone and θ is the polar angle of the jet direction. $E_T(2)$ refers to the transverse energy of the second highest jet, and so forth.

For this analysis, two data samples were used, one with a modest fraction of $t\bar{t}$ events and one that is an enriched subset. Table I gives the names and characteristics for the two data sets along with the number of events and background fractions. The first data set (Standard 3-jet) is composed of events with the W signature of an isolated charged lepton (electron or muon) with $P_T > 20$ GeV/c in the central region of the detector ($|\eta| < 1.0$) and missing transverse energy ($\not\!\!E_T$) greater than 20 GeV [15]. The lepton isolation I is defined as the extra transverse energy in a cone of R = 0.4 centered on the lepton divided by the lepton P_T. A charged lepton is considered isolated if $I < 0.1$. In addition at least three jets are required to have observed calorimeter $E_T > 15$ GeV and $|\eta| < 2.0$; any additional jets used in the analysis are required to have observed $E_T > 8$ GeV and $|\eta| < 2.4$. Events with identified dileptons are removed. In addition events with e^+e^- or $\mu^+\mu^-$ pairs that satisfy less stringent lepton identification requirements but that have an invariant mass between 75 and 105 GeV/c^2 are treated as $Z \to l^+l^-$ decays and removed. Events with an electron consistent with being from a photon conversion are also removed. The data sample fulfilling these requirements consists of 322 events and is dominated by non-$t\bar{t}$ events.

The second data set (SVX b-tagged) satisfies the same requirements and additionally one of the jets must be tagged as a b-jet candidate using the SVX detector. Decays of long-lived b states can be identified by the presence of a secondary vertex that is displaced from the primary vertex. A displaced vertex requires three or more tracks satisfying loose track requirements, or two tracks with stringent track and vertex requirements. This data set consists of 34 events and is enriched in top.

III. MODELS OF $t\bar{t}$ PRODUCTION AND DECAY

The predicted properties of $t\bar{t}$ events are calculated using Monte Carlo generators corrected for the effects of the CDF detector response and reconstruction algorithms [16] using a detailed simulation. The same cuts that are used for the data are applied to the Monte Carlo samples. Unless otherwise stated, the top mass is set to 175 GeV/c^2 consistent with the measurements by CDF [10] and D0 [11].

The available event generators start with the leading order matrix element and use QCD parton showers to simulate higher orders. Hard Next-to-Leading-Order corrections to the tree-level matrix elements have been shown not to affect the shape of the inclusive top quark distributions [17]. Parton fragmentation is a two step process: the parton shower (gluon radiation) with a cutoff followed by non-perturbative hadronization. Finally a soft underlying event is added. The main difference between generators for this study is the modeling of the gluon radiation associated with the parton evolution.

Before examining the data, three different $t\bar{t}$ Monte Carlo programs are compared. These are HERWIG [18] version 5.6, PYTHIA [19] version 5.7 and ISAJET [20] version 7.06. With all three programs the MRSD0′ structure functions were used. In HERWIG the hard scattering is followed by color coherent parton shower evolution, cluster hadronization, and an underlying event model based on data collected by the UA5 collaboration in $p\overline{p}$ collisions at $\sqrt{s} = 200 - 900$ GeV [21]. PYTHIA provides color coherent shower evolution, string hadronization, and an underlying event model based on multiple parton scattering. ISAJET provides incoherent shower evolution, independent fragmentation of the outgoing partons, and an underlying event model based on the AGK cutting rules [22]. For this study only the shapes of distributions are utilized; no use is made of the absolute normalization.

The predictive ability of these Monte Carlo generators has been studied on larger samples of QCD multijet events at the Fermilab Tevatron collider. The suppression of soft gluon radiation in certain regions of phase space due to color coherence in parton showers has been observed by studying soft jets in hard multijet events [23]. HERWIG and PYTHIA which both implement color coherence in parton showers are expected to reproduce the data better than ISAJET which does not.

IV. BACKGROUNDS

The Standard 3-jet sample is dominated by backgrounds which can be divided into three categories: events from the QCD production of a W or Z plus jets (QCD W/Z + jets), events that contain no real W or Z (non-W/Z), and events from processes such as WW or single top production (Miscellany). The kinematic properties of the first category are simulated, but the rate is determined from the data. The non-W/Z events have a much smaller rate that is also determined from the data. The Miscellany category has a still smaller rate which is determined by Monte Carlo calculation of the individual contributions.

The kinematic characteristics of the QCD W/Z + jets background are modeled with VECBOS [24], a leading order Monte Carlo program which describes the direct production of a W recoiling against quarks and gluons. Parton shower evolution and hadronization are implemented using the models contained in HERWIG [18]. For the present study, VECBOS calculations used the MRSD0′ structure functions and two factorization and renormalization scales which represent reasonable extremes: $Q^2 = < \mathrm{P_T} >^2$, where $\mathrm{P_T}$ is the transverse momentum of the partons recoiling against the W, and $Q^2 = \mathrm{M}_W^2$. The former produces a softer jet $\mathrm{P_T}$ spectrum than the latter. The background distributions are generated by mixing equal luminosity samples of VECBOS Monte Carlo events with the two different Q^2 scales. Differences between the two background samples represent a measure of the sensitivity to the Q^2 scales. Divergences are avoided by restricting the phase space of the partons to $\mathrm{P_T} > 8$ GeV/c, $| \eta | < 2.5$, and separation $\Delta\mathrm{R} = \sqrt{\Delta\eta^2 + \Delta\phi^2} > 0.4$. These cuts were chosen to accept partons that might fragment into a jet satisfying the requirements of this analysis. The kinematically similar Z + jets background where one charged lepton from the decay $Z \to l^+l^-$ is not identified makes up about 7% of this category. QCD W/Z + jets accounts for about 85% of the total background in the Standard 3-jet sample. A more detailed study of the modeling of QCD W + jets data by VECBOS, including lower jet multiplicities, can be found in Reference [25].

In order to predict SVX tagging rate for the QCD W/Z + jets events, it is necessary to know the heavy flavor content of the jets. This was calculated with the procedure detailed in Reference [3], using both exact matrix element calculations [24, 26] and HERWIG results for the production of heavy quarks inside jets. For the Standard 3-jet sample, the fraction of the QCD W/Z + jets background that contains $Wb\overline{b}$, $Wc\overline{c}$,

or Wc is determined to be about 15%. Studies of the Monte Carlo events generated with VECBOS forced to use only diagrams that contribute to heavy flavor production indicate that they are kinematically similar to the normal mix of events generated by VECBOS.

The next largest background is the non-W/Z, which is due to fake leptons or QCD production of $b\overline{b}$ where the electron or muon comes from the decay of one of the b hadrons. The non-W/Z rate is measured by studying the data as a function of lepton isolation I and $\not\!\!E_{\rm T}$. It corresponds to about 10% of the total background in the Standard 3-jet data set. In these events the P_T spectra of the jets are slightly harder than in events generated by VECBOS while the charged lepton P_T and missing transverse energy spectra are both softer. The remaining 5% is Miscellany consisting of events with a WW, WZ, or ZZ; events with $Z \to \tau^+\tau^-$; and single-top production.

After accounting for the non-W/Z and Miscellany backgrounds, the numbers of QCD W/Z + jet events and $t\overline{t}$ events are readily determined from the predicted SVX tagging rate for each and the number of events in the two data sets. The fraction of $t\overline{t}$ in the 322 event Standard 3-jet data set is determined to be $20 \pm 4\%$.

For the 34 SVX b-tagged events, the $t\overline{t}$ fraction is $75 \pm 5\%$. In this data set, the QCD W/Z + jets account for only about 65% of the background. Because the mistag rate for light flavor is low, most of the tagged QCD W/Z + jets background contains heavy flavor. The non-W/Z component of the background increases to about 20% due to its large $b\overline{b}$ content and the remaining Miscellany now makes up 15% of the background. Figure 1 graphically summarizes the $t\overline{t}$ content and the background composition of both data sets.

When comparing the kinematic properties of $t\overline{t}$ candidate events in the data to theoretical predictions, the studies presented here model all background components with events generated by the VECBOS W + jets Monte Carlo program. In previous studies, the background distributions for some kinematic variables were successfully simulated using this approximation [6, 7, 10]. Agreement with the data depends both on the ability of VECBOS to correctly calculate the W/Z + jets process and on the size of the other background components being small and/or not too different kinematically from W/Z + jets. In Section VII it is shown that the effects of simulating the non-W/Z events (the majority of the other backgrounds) with VECBOS are small–particularly for the SVX b-tagged sample.

Figure 1 puts into perspective the modeling of the background. To the extent that VECBOS models all the background in the Standard 3-jet sample, it should satisfactorily model the smaller fractions of the total number of events that are non-W/Z and Miscellany in the statistically less discriminating SVX b-tagged sample. The comparisons that follow between data and Monte Carlo predictions for the SVX b-tagged sample should test the $t\bar{t}$ generators.

V. KINEMATIC VARIABLES

In this section the kinematic variables used in this study are described. These variables are functions of the momenta and energies of the leptons and jets in the event. The charged leptons are well measured [3] compared to the jets. A jet's energy and momentum are determined from the scalar and vector sums, respectively, of the calorimeter tower energies inside a cone of R = $\sqrt{\Delta\eta^2 + \Delta\phi^2} = 0.4$ centered on the jet direction. A rapidity and energy-dependent correction factor is applied which accounts for the calorimeter nonlinearity and the reduced detector response at detector boundaries [14]. A correction is made for the energy which is radiated out of the jet reconstruction cone [27]. Finally, subtractions to the jet energy are made for the underlying event and any other interactions observed in the same beam crossing. The transverse momentum of the neutrino expected from the $W \rightarrow l\nu$ decay is set equal to the missing transverse energy in the event. The longitudinal momentum of the neutrino is determined by constraining the neutrino and charged lepton to the mass of the W which usually leads to two real solutions. The solution with the smallest value of $\mid P_Z \mid$ is the most probable for $t\bar{t}$ events and is used for those variables that require P_Z of the neutrino.

It is useful to divide the kinematic variables into two classes: those that depend primarily on the energy in the event and those that are more a function of the angles between the leptons and jets. The energy variables are more sensitive to the top quark mass and have the property that the mean value of the variable is usually greater for the $t\bar{t}$ signal than for the QCD W/Z + jets background. Table II lists the primary energy variables with a short description. Most use only the transverse components of the momentum because the transverse components discriminate better between the $t\bar{t}$ signal and the QCD background than

the longitudinal components. The variable Mass(W+4 jets) which does use longitudinal momentum is also of interest because it is approximately the mass of the $t\bar{t}$ system. Any sum over jets is limited to the five highest E_T jets.

Table III lists the primary angular variables with a short description. Polar angle variables can separate signal from background since top quarks and their decay products are produced more centrally. Distributions depending on ϕ have a similar ability to discriminate because $t\bar{t}$ events are more circular than the background. Aplanarity is a useful combination of the angular variables (θ, ϕ).

VI. STUDIES OF THE MONTE CARLO GENERATORS

In the remainder of this paper, the distributions of the kinematic variables are compared among different $t\bar{t}$ generators, QCD background, and the data. Before comparing with the data, the characteristics of the generators are studied using Monte Carlo samples which have been run through the CDF detector simulation and the leptons and jets are reconstructed using the same algorithms as the data. The $t\bar{t}$ programs are compared for consistency over a large selection of variables. Particular note is made of the effects of gluon radiation. The variables are examined for their sensitivity to top mass, ability to discriminate between $t\bar{t}$ and the QCD background, and sensitivity to any tagging bias.

A. General Features using Moments

To simplify the presentation of the results, we characterize the kinematic distributions by their first two moments.

1. The First Two Moments

Figure 2 shows the predicted means of four variables for the Standard 3-jet data set versus the value of the top mass used in the Monte Carlo programs. The points indicate the means for both HERWIG and PYTHIA; linear fits to the means as a function of top mass are shown for all three generators. These plots show good

consistency between the $t\bar{t}$ generators; the variables with larger slopes in general are more sensitive to the mass of the top quark.

The hatched horizontal bands on the plots show the VECBOS prediction for each variable. As expected, the kinematic distributions obtained using this QCD W + 3 jet program are insensitive to the top quark mass. The widths of the VECBOS bands show the variation due to two quite different Q^2 scales: $< \mathrm{P_T} >^2$ and M_W^2; they provide an estimate of the uncertainty in the VECBOS predictions.

The results from linear fits to the first two moments, the means and rms's, for a more extensive selection of variables evaluated at a top mass of 175 GeV/c^2 are summarized in Table IV and Table V for all three $t\bar{t}$ generators.

Table VI compares the predicted means from HERWIG for the Standard 3-jet and SVX b-tagged samples. The comparison shows very little bias due to b-tagging in $t\bar{t}$ events. For the SVX b-tagged sample, the means of the jet $\mathrm{P_T}$ variables are slightly higher and the events are slightly more central, primarily due to the limited η coverage available for b-tagging.

In Figure 3, we plot (Mean($t\bar{t}$)-Mean(QCD bkg.))/rms(QCD bkg.) which constitutes a measure of how efficient a variable is at differentiating $t\bar{t}$ events from the QCD background. Variables with large values of this quantity differentiate better than variables with small values. $\mathrm{P_T}(3)$ and H both discriminate well, Aplanarity more modestly, and $\mathrm{P_T}$(electron) poorly.

Figure 4 puts into perspective the precision of measurements made from the data relative to the features of the moments plots shown in Fig. 2. The bands show the Monte Carlo predictions for the mean as a function of the top mass for the expected mixture of $t\bar{t}$ and QCD background. The widths of these bands represent the uncertainty in the top fraction for each sample. The points are the data.

2. Top Mass Sensitivity of the Variables.

An important aspect of each variable is its sensitivity to the mass of the top quark. Mass sensitivity is a source of systematic uncertainty when comparing data with Monte Carlo predictions (see Section VII). Mass sensitivity also provides guidance as to which variables might be suitable for an alternative top mass

measurement and which variables might be able to kinematically separate $t\bar{t}$ events from the QCD background with less biasing of a mass measurement.

For any variable a likelihood fit of the data to the predicted distribution parameterized as a function of the top quark mass would yield a measurement of this mass. If the distribution of the variable were Gaussian and there were no background, the statistical uncertainty in the fitted top mass would be the (rms/slope)/$\sqrt{\mathrm{N}}$ where slope is the variation of the mean as a function of generator top mass and N is the number of data events. Variables that are sensitive to the top quark mass have a small value of the quantity "rms/slope". Because the distributions are not Gaussian and in general have large tails, the rms overestimates the effective widths that determine the mass resolution. Backgrounds will also affect variables differently. Therefore the quantity "rms/slope" is only a rough guide to the mass sensitivity of a variable.

Table VII gives the "rms/slope" for a selection of energy variables. Variables that depend only on the lepton and neutrino from the decay of the W have only a small dependence on the mass of the top quark. The jet $\mathrm{P_T}$ distributions are more sensitive to the top mass with the sensitivity increasing for higher $\mathrm{P_T}$ jets. The variables with the greatest sensitivity to mass of the top quark are H and Mass(W + 4 jets). Variables that are more sensitive to angles or the shape of an event such as aplanarity have little sensitivity to top mass and are not listed in the table.

Events with 4 or more jets can be fit to a $t\bar{t} \to Wb W\bar{b}$ hypothesis to provide a sample that is more sensitive to top mass than any of the simple kinematic variables in this analysis [3,10]. It is estimated that the reconstructed mass from fits to the $t\bar{t}$ hypothesis gives a measurement of the top mass that has a statistical uncertainty 10% to 20% smaller than a measurement using the H variable.

B. The Full Distributions

The full distributions are useful in detailing differences between the $t\bar{t}$ Monte Carlo programs. Kinematic distributions for the SVX b-tagged sample corrected for detector effects were generated using the three $t\bar{t}$ programs with a top mass of 175 GeV/c^2. Because parton shower effects are expected to be a major contributor to generator differences, the PYTHIA program was also run with final state radiation (FSR)

and/or initial state radiation (ISR) turned off. Understanding the pattern of gluon radiation is an important theoretical goal that has an impact on the understanding of $t\bar{t}$ production and the accurate determination of the top mass [28].

1. Statistical tests

The sample sizes for this comparison were 5522 events for HERWIG, 4044 events for PYTHIA, 1855 events for ISAJET, 3759 events for PYTHIA with no ISR, and 4244 events for PYTHIA with no FSR. Note that 5000 $t\bar{t}$ events with an SVX b-tagged jet correspond to an integrated luminosity of about 20 fb^{-1}.

The different gluon radiation models represented by these samples were compared by performing Kolmogorov-Smirnov (KS) tests on the distributions relative to the ones predicted by regular PYTHIA. The KS probabilities are calculated using the maximum difference between properly normalized integrals of the two distributions and are designed to give a uniform probability between 0 and 1 if the two distributions come from the same parent distribution. For simplicity the events in this study are binned, which means that the difference between the two integrals are checked only at bin boundaries. Since, in general, the maximum deviation will not occur at a bin boundary, the probability that is returned will always be an upper limit for the unbinned KS probability. For the binning and sample sizes in this paper, the average KS probability will range from 0.60 to 0.65 if the two distributions have the same parent; likewise, about 6% of the time the KS test will return a probability of less than 0.10 and about 0.4% of the time a probability less than 0.01. Table VIII summarizes the probabilities from the binned KS tests between PYTHIA and the other generators for a diverse selection of 15 variables.

The KS tests comparing HERWIG and PYTHIA indicate that they are difficult to distinguish given the statistical power of the Monte Carlo samples. The average KS probability for the ensemble of 15 variables is 0.49 which is lower than the expected average of 0.62 by about 1.3 standard deviations after taking into account the correlations between the variables.

The differences between PYTHIA and ISAJET are too large to be explained by correlations or fluctuations. For the same set of 15 variables the average probability is 0.23 compared to the expected average of 0.62. In

addition there are seven variables with probability less than 0.10 compared to the expected number of one. However, the differences are not large enough to be seen easily in the data.

Turning off ISR affects variables that depend on the longitudinal components of the momenta or the P_T of the lower energy jets. The average probability for KS tests between PYTHIA and PYTHIA with no ISR is 0.23 and there are 8 variables with probability less than 0.10 and 4 with probability less than 0.01. The agreement is poor.

Turning off FSR has the largest effect on the probabilities. The lack of harder gluon radiation affects jet-jet separation. The lack of softer radiation increases the fraction of jet energy deposited in a cone of 0.4 thereby increasing the jet P_T which has been corrected assuming a less collimated jet. The average probability is 0.10 and ten variables have probability less than 0.01

These comparisons using the KS test indicate that for some variables the Monte Carlo distributions are sensitive to gluon radiation modeling. They are also consistent with the expectation that ISAJET, which does not implement color coherence, is more different from HERWIG and PYTHIA than they are from one another.

2. Variables with Sensitivity to Gluon Radiation

Three types of variables were found that have some sensitivity to gluon radiation while having limited dependence on the mass of the top quark and the jet energy scale. One type depends on the amount of energy that goes into extra jets, another on the separation of jets, and the last on the widths of jets. Comparisons with the data puts into perspective the significance of any differences.

An example of the first type of variable is the fraction of events with a 5th jet. If there is no gluon radiation, there will be at most four jets in an event (except for the very few cases where the jet clustering algorithm divides one jet into two jets). The 34 event SVX b-tagged sample has 11 events containing a 5th jet with $E_T > 8$ GeV and $| \eta | < 2.4$. Table IX shows the predicted fractions of such events for $t\bar{t}$ alone and for the expected mixture of $t\bar{t}$ and QCD background. The last column of the table converts the fractions to events.

The $t\bar{t}$ events with at least 5 jets have roughly equal contributions from ISR and FSR; for the extreme case of no ISR and no FSR, the last row of the table shows a negligible number of events. The presence of additional $p\overline{p}$ interactions in an event can contribute additional energy to jets that is not modeled by Monte Carlo. Reasonable variations on the correction applied to jets for this effect cause one jet to fall below the E_T threshold reducing the number of 5 jet events from 11 to 10. This gives an estimate of the systematic uncertainty due to this effect. The data are in good in agreement with predictions for the expected mixture of QCD background and HERWIG, PYTHIA, or ISAJET. The probability that the number of data events is compatible with the prediction for PYTHIA with no ISR and no FSR is less than 10^{-5}, but there are not yet enough data to fully explore interesting levels of gluon radiation.

The other two types of variables are only sensitive to FSR. An example of the second type is the minimum separation in ΔR among pairs of jets (because gluon radiation results in more jets with smaller separation). Figure 5 shows the distributions for this variable. The top plot shows PYTHIA compared with HERWIG and ISAJET. The middle plot shows the effects of turning off FSR and ISR in PYTHIA. And the lower plot shows the expected mixture of $t\bar{t}$ and QCD background compared with the QCD background only and the 34 SVX b-tagged events. The mean of the data is less than one standard deviation from both the Monte Carlo prediction using regular PYTHIA or HERWIG and the prediction using PYTHIA with no FSR. Some other variables of this type, such as the minimum di-jet mass, are a little more sensitive to FSR than the minimum jet-jet separation, but they are also more sensitive to the top mass and jet energy scale. More data would sharpen the comparison.

The third type of variable depends on the widths of the jets. A simple measure of the jet width is the ratio of transverse energy in a cone of 0.4 to the transverse energy in a cone of 0.7. Gluon radiation results in a smaller fraction of energy in a cone of 0.4. Because both the ratio and the correction to the ratio for the underlying event and multiple interactions are functions of jet energy, it is useful to consider separately the jets in different energy intervals. Figure 6 shows this ratio for jets with an observed E_T between 30 GeV and 60 GeV which is the most sensitive range. As expected, PYTHIA with no FSR is markedly narrower and has a higher mean than either regular PYTHIA or HERWIG. The data are slightly broader and lower

in mean than regular PYTHIA or HERWIG, but still less than two standard deviations from the extreme case of no FSR. The distribution of same ratio for jets in the observed E_T range between 15 GeV and 30 GeV agrees better with the no FSR prediction, but has fewer entries, larger systematic uncertainties, and is consistent with all predictions.

No variables were found with comparable sensitivity to initial state gluon radiation although some variables with a polar angle dependence do have a small sensitivity.

C. Generator Study Conclusions

Since differences between HERWIG and PYTHIA are not readily observable using the statistical power of several thousand events, HERWIG is arbitrarily chosen as the default $t\bar{t}$ Monte Carlo program. ISAJET samples with slightly less statistical power showed definite differences that appear associated with the parton shower implementation. PYTHIA with no FSR or no ISR showed differences with regular PYTHIA which occurred for specific classes of variables that are sensitive to gluon radiation. However, the size of the data sample is not large enough to set useful limits on gluon radiation.

VII. COMPARISON OF MEANS

To facilitate the graphical comparisons of many variables, their means are plotted in the following set of figures. Figure 7 exhibits the features of these figures for a single variable. The left end of the line represents the mean of the variable for QCD background events and the right end of the line the mean for $t\bar{t}$ events. The data, represented by the solid circle, is plotted at a position along the line proportional to the value of its mean relative to the means for the QCD background and $t\bar{t}$ production. A vertical shaded band indicates the expected position of the data mean based on the measured fraction of top events from b-tagging and background studies. The expectation is that the circles representing the data will fall near the shaded band. If the data is more background-like then the circles will be left of the band, more top-like and the circles will be to the right of the band.

The means for the 322 event Standard 3-jet sample are displayed in Figure 8. The vertical shaded band centered on 20% shows the expected top fraction and its uncertainty. Since this sample is mostly background, it is more a check that VECBOS is a good predictor of the QCD background than that HERWIG is a good predictor of $t\bar{t}$ kinematics. The lengths of the arrows on the plot represent the statistical uncertainty in the data and are a measure of how well each variable discriminates between the QCD background and $t\bar{t}$ production. Variables with shorter arrows have more discriminating power. The variable with the best discriminating power is $P_T(3)$ + $P_T(4)$ followed by $\sum P_T(\text{jet})$. The data are presented in tabular form in Table X. No significant deviations from the predicted means are observed.

The means for the 34 event b-tagged sample are shown in Figure 9. The vertical shaded band centered at 75% top represents the estimated top fraction in these events. Since this data sample is mostly $t\bar{t}$, it is more sensitive to the predictive power of HERWIG than of VECBOS. For the SVX b-tagged sample the variable with the best discriminating power between the QCD background and $t\bar{t}$ production is $P_T(3)$ + $P_T(4)$ followed by H. The data are presented in tabular form in Table XI.

The primary purpose of these plots is to show the consistency of the data with the Monte Carlo predictions constrained by the measured $t\bar{t}$ fraction and the previously measured top mass of 175 GeV/c^2. One caveat concerning these plots is that there are significant correlations between many of the variables. For example, in events where the t and $\bar{t}$ are produced at high P_T, the average values of all of the energy variables will in general be larger. Because the variables are correlated, they cannot be simply combined to yield a more sensitive comparison of the observed and predicted means.

A. Systematic Uncertainties

The main systematic uncertainties are discussed in this section. Two important items, the mass of the top quark and the shapes of the QCD background spectrum, were discussed in Section VI. The other major source of uncertainty, the jet energy scale [10], is examined below. Other less important contributors to the systematic uncertainty in the Monte Carlo predictions include the parton distribution functions and the b-tagging bias. The effect of the principal systematic uncertainties on the means of the Monte Carlo

distributions are summarized in Tables XII, XIII for the regular set of variables.

One measure of the uncertainty in the VECBOS distributions is the difference in predictions for two reasonably extreme Q^2 scales: $< \mathrm{P_T} >^2$ and M_W^2. The shifts in the means correspond to the widths of the cross-hatched VECBOS bands in Figure 2. The half-widths of these bands are listed as VECBOS systematic uncertainties in Tables XII, XIII.

The systematic uncertainty due to a 4.8 GeV/c^2 shift in the top quark mass is included in Tables XII, XIII. This corresponds to the statistical uncertainty in the CDF measurement of the top mass in the lepton plus jets channel [10]. No contribution due to the systematic uncertainty in this measurement is included since it is dominated by jet energy scale effects which are considered separately (see below). Reductions to the uncertainty in the top quark mass from the inclusion of results from other channels and other experiments make this systematic error an upper limit.

The jet energy scale systematic affects the predictions for both QCD background and $t\bar{t}$. It is a measure of how well the fully reconstructed jet energy provided by the Monte Carlo and detector simulation models that for the data. The following four quantities contribute to this difference: the stability of the calorimeter gain (about 1%); the modeling of the variation in the relative response of the detector as a function of η (varies from 0.2% and 4.0%); the measured absolute energy response of the central calorimeter (about 3%); and the Monte Carlo modeling of the fraction of the energy in a jet that is deposited in the clustering cone of 0.4 (1% to 6%). These four quantities are added in quadrature and the resulting uncertainty is used to shift the energy in the clustering cone on a jet-by-jet basis for large Monte Carlo samples of events. The shift in the jet energy varies from 10% for the lowest $\mathrm{P_T}$ jets to 3% for the higher $\mathrm{P_T}$ jets and on average is about 5%. The resulting shifts in the means of selected variables are shown in Tables XII, XIII for both VECBOS and HERWIG $t\bar{t}$.

The effect of any of the individual systematic errors on the Monte Carlo prediction for the expected mix of VECBOS plus HERWIG $t\bar{t}$ is smaller than the statistical uncertainty in the data. For the Standard 3-jet sample, which tests primarily the modeling of the background by VECBOS, the total uncertainty for jet $\mathrm{P_T}$ variables due to the systematic errors examined in this section are typically comparable to or slightly

less than the statistical uncertainty in the data; the systematic uncertainty for other variables is smaller. For the SVX b-tagged sample, which tests primarily the modeling of $t\bar{t}$ production by HERWIG, the total systematic uncertainty for the jet P_T variables is typically half of the statistical uncertainty in the data; the systematic uncertainty for other variables is smaller. These systematic uncertainties are small enough to allow a meaningful comparison between the Monte Carlo prediction and the data.

VIII. COMPARISON OF DISTRIBUTIONS

In the previous section it was shown that the means of the distributions agreed with the predictions for the expected mixture of QCD background and $t\bar{t}$. Figures 10-17 compare the shapes of the kinematic distributions observed in the data with Monte Carlo predictions, again using VECBOS to model the QCD background and HERWIG to model $t\bar{t}$ production. There is one figure for each variable; the top two plots in each figure are for the Standard 3-jet sample and the bottom two plots are for the SVX b-tagged sample.

The plots on the left are differential plots showing the number of events versus the value of the variable. The points with error bars are the data and the shaded area is the prediction for the expected mixture of QCD background and $t\bar{t}$. The Monte Carlo histograms are normalized to the number of observed events. In general the data have the same shape as the shaded area.

The plots on the right are integral significance plots. The horizontal axis is still the value of the variable, but the vertical axis is the difference between the integral of the data above that point and the predicted integral for a pure background sample divided by the statistical uncertainty in the integral of the data. These integrals, when properly normalized, become the fraction of the events above the evaluation point and are denoted as "Frac(data)" and "Frac(VECBOS)." The ordinate can be expressed in terms of these fractions:

$$\text{Ordinate} = \frac{\text{Frac(data)} - \text{Frac(VECBOS)}}{\sigma}$$

where

$$\sigma = \sqrt{\frac{(\text{Frac(mix)} + \frac{1}{\text{N}})(1 - \text{Frac(mix)} + \frac{1}{\text{N}})}{\text{N}}}$$

"Frac(mix)" is the fraction of the expected mixture of VECBOS and HERWIG $t\bar{t}$ above the point being plotted and N is the total number of events in the data sample. In the limit of large N, the expression for σ becomes the more familiar $\sqrt{\mathrm{Frac(mix)(1-Frac(mix))/N}}$.

The solid points are the data and the shaded band shows the Monte Carlo prediction for the expected mixture of VECBOS and HERWIG $t\bar{t}$ evaluated for a top quark mass of 175 GeV/c^2. The width of the band quantifies the difference between the two Q^2 scales for VECBOS of $< P_{\mathrm{T}} >^2$ and M_W^2. The hatched band is the equivalent prediction for a top quark mass of 185 GeV/c^2. Deviations from the predicted behavior are contained in the vertical difference between the data points and the bands; this difference is in units of the statistical uncertainty in the data. The significance of the difference between the data integral and the prediction band is easily read off of the plot for any value of the variable. Integral plots are sensitive to the same differences in shape as the KS test and are useful when studying the tails of distributions where statistics are low. Note that within integral plots there are large correlations between adjacent points.

Figures 10 and 11 show the distributions for $\mathrm{P_T}$(lepton) and $\not\!\!E_{\mathrm{T}}$. The predictions are similar for both VECBOS and the expected mixture of VECBOS and HERWIG $t\bar{t}$, but the data agree better with the latter predictions. Figures 12 and 13 display the $\mathrm{P_T}$ distributions for the highest $\mathrm{P_T}$ jet and the third highest $\mathrm{P_T}$ jet. Figures 14 and 15 show $\mathrm{P_T}(3)$ + $\mathrm{P_T}(4)$ and H, both of which depend strongly on jet $\mathrm{P_T}$. For these variables the data are consistent with the predictions for the expected mixture of VECBOS and HERWIG $t\bar{t}$ and differ by several σ from the predictions for pure VECBOS. Figure 16 shows the Mass(W+4 jets) which is a good approximation to the invariant mass of the $t\bar{t}$ system. This is a particularly interesting variable in the context of non-standard model theories which postulate the existence of high mass $t\bar{t}$ resonances [8]. There is no indication in Figure 16 of extra production at high $t\bar{t}$ invariant masses. Figure 17 shows the aplanarity, which has little dependence on top mass as evidenced by the consistency between the shaded and hatched bands.

In order to be more quantitative in the comparisons, some standard statistical tests have been applied. For each differential histogram, a χ^2 is calculated from the comparison of the distribution observed in the data with the predicted one and the corresponding probability evaluated. This probability should be uniformly

distributed between 0 and 1 if the predicted distribution is consistent with being the parent population for the data. The χ^2 and corresponding probability are calculated using the binning that is shown in Figures 10-17 and with similar binning for those variables not accompanied by a plot.

In addition the KS test is used to determine the probabilities that the integral distributions of the data are consistent with the predictions for the expected mixture of VECBOS and HERWIG $t\bar{t}$. The KS test is done using binned data with binning that is finer than that shown in Figures 10-17 (typically 50-100 bins). The binning causes the normally uniform probability distribution between 0 and 1 to be skewed to larger values with an average probability between 0.6 and 0.65 depending on the sample size and the effective number of bins.

Table XIV shows both the χ^2 and binned KS probabilities of the two data sets for a diverse set of 15 variables. The expected statistical uncertainty in the average probability using either test is slightly less than 0.08 for 15 uncorrelated variables; however, correlations between similar variables in the same event increase the expected statistical uncertainty in the average probability to about 0.10 for the specific set of 15 variables. For the 322 event Standard 3-jet sample, which is mostly non-$t\bar{t}$ background, the average χ^2 probability is 0.41 and the average KS probability is 0.50. Both averages are acceptable; they are 1.3 σ or less from their expected values of 0.50 and 0.63 respectively. For the 34 event SVX b-tagged sample the average χ^2 probability is 0.56 and the average KS probability is 0.75. The larger values of these average probabilities indicate good agreement with Monte Carlo predictions; they are 1.3 σ or less from their expected values of 0.50 and 0.62 respectively. Since this sample is mostly $t\bar{t}$, this is primarily a check that the standard model correctly describes $t\bar{t}$ production.

IX. CONCLUSIONS

Monte Carlo generators for $t\bar{t}$ production were examined for consistency with particular attention paid to the effects of gluon radiation. Kinematic distributions of simulated events corrected for detector response were in good agreement for HERWIG and PYTHIA, both of which implement color coherence in parton showers. Differences were apparent in the ISAJET predictions for variables expected to be sensitive to gluon

radiation. The sizes of the dominant components in the data, the QCD W/Z + jets background and the $t\bar{t}$ signal, were determined from the b-tagging efficiencies for each and the b-tagging rates observed in the data. Small rates or similarities in the other background components indicated that the VECBOS W + jets generator was suitable for modeling the kinematic characteristics of all the background. Individual kinematic variables were examined for sensitivity to the top quark mass and their utility in discriminating between $t\bar{t}$ and the QCD background.

Using HERWIG to simulate standard model $t\bar{t}$ production and VECBOS to describe the background, kinematic distributions in the data were compared to Monte Carlo predictions using both plots and standard statistical tests. The selection of variables was chosen to be sensitive to different aspects of $t\bar{t}$ production. These included the P_T of the higher P_T jets, the lower P_T jets, the b-tagged jets, the leptons, and sums of these. Other variables were the Mass(W +4 jets) which contains longitudinal energy, shape variables such as aplanarity, centrality variables such as $\cos(\theta^*)_{\max}$, and variables sensitive to the separation of jets. The Monte Carlo predictions used the measured value of the top quark mass and the $t\bar{t}$ fractions determined from b-tagging and background studies. Since the 322 event Standard 3-jet sample is only 20% $t\bar{t}$, the comparison for it primarily shows the accuracy with which the background is modeled by VECBOS; the data are consistent with the Monte Carlo predictions. The 34 event SVX b-tagged sample, which is 75% $t\bar{t}$, primarily tests the accuracy of the HERWIG $t\bar{t}$ generator. The agreement between the SVX b-tagged data and Monte Carlo predictions indicates that the standard model leading order $t\bar{t}$ matrix element with color coherent parton shower evolution reproduces the data well.

We thank the Fermilab staff and the technical staffs of the participating institutions for their vital contributions. This work was supported by the U.S. Department of Energy and National Science Foundation; the Italian Istituto Nazionale di Fisica Nucleare; the Ministry of Education, Science and Culture of Japan; the Natural Sciences and Engineering Research Council of Canada; the National Science Council of the Republic of China; the Swiss National Science Foundation; and the A. P. Sloan Foundation.

[1] CDF Collaboration, F. Abe *et al.*, Phys. Rev. Lett. **74**, 2626 (1995).

[2] D0 Collaboration, S. Abachi *et al.*, Phys. Rev. Lett. **74**, 2632 (1995).

[3] CDF Collaboration, F. Abe *et al.*, Phys. Rev. D **50**, 2996 (1994);
Phys. Rev. Lett. **73**, 225 (1994).

[4] D. Amidei *et al.*, Nucl. Instrum. Methods A **350**, 73 (1994);
P. Azzi *et al.*, *ibid.* **360**, 137 (1995).

[5] CDF Collaboration, F. Abe *et al.*, Phys. Rev. Lett. **80**, 2773 (1998).

[6] CDF Collaboration, F. Abe *et al.*, Phys. Rev. Lett. **75**, 3997 (1995).

[7] CDF Collaboration, F. Abe *et al.*, Phys. Rev. D **51**, 4623 (1995);
F. Abe *et al.*, Phys. Rev. D **52**, R2605 (1995).

[8] C.T. Hill, Phys. Lett. **B345**, 489 (1995);
C.T. Hill and S.J. Parke, Phys. Rev. D **49**, 4454 (1995);
E. Eichten and K. Lane, Phys. Lett. **B327**, 129 (1994);
R. Casalbuoni *et al.*, Z. Phys. C **69**, 519 (1996);
T. Gehrmann, W.J. Stirling, Phys. Lett. **B381**, 221 (1996).

[9] G.L. Kane and S. Mrenna, Phys. Rev. Lett. **77**, 3502 (1996).

[10] CDF Collaboration, F. Abe *et al.*, Phys. Rev. Lett. **80**, 2767 (1998).

[11] D0 Collaboration, B. Abbott *et al.*, Phys. Rev. D **58**, 052001 (1998).

[12] M. Binkley in Proceedings of the 10th Topical Workshop on Proton-Antiproton Collider Physics, Batavia Illinois, 1995, edited by R. Raja and J. Yoh (AIP Press).

[13] A. Beretvas, Int. J. Mod. Phys. A **11**, 2233 (1996).

[14] CDF Collaboration, F. Abe *et al.*, Phys. Rev. D **45**, 1448 (1992).

[15] In the CDF coordinate system, θ is the polar angle with respect to the proton beam direction and ϕ is the

azimuthal angle. The pseudorapidity η is defined as -ln tan(θ/2). The transverse momentum of a particle is defined as P_T = P sin(θ) where P is the particle momentum. The missing E_T is defined as the negative of the vector sum of all the transverse energies in the event.

[16] C. Newman-Holmes and J. Freeman, in Proceedings of the Workshop on Detector Simulation for the SSC, Argonne Il. 1987, edited by L.E. Price, ANL-HEP-CP-80-51, pp 190, 285.

[17] S. Frixione, M.L. Mangano, P. Nason and G. Ridolfi, Phys. Lett. **B351**, 555 (1995).

[18] G. Marchesini and B.R. Webber, Nucl. Phys. B **310**, 461 (1988).
G. Marchesini *et al.*, Comput. Phys. Commun. **67**, 465 (1992).

[19] H. Bengtsson and T. Sjöstrand, Comput. Phys. Commun. **46**, 43 (1987).

[20] F. Paige and S.D. Protopopescu, BNL Report No. 38034, 1986 (unpublished).

[21] UA5 Collaboration, G.J. Alner *et al.*, Nucl. Phys. B **291**, 445 (1987).

[22] V.A. Abramovskii, O.V. Kancheli and V.N. Gribov in Proc. XVI Intern. Conf. on High Energy Physics, NAL 389 (1972).

[23] CDF Collaboration, F. Abe *et al.*, Phys. Rev. D **50**, 5562 (1994).

[24] F.A. Berends, W.T. Giele, H. Kuijf, and B. Tausk, Nucl. Phys. **B357**, 32 (1991).

[25] CDF Collaboration, F. Abe *et al.*, Phys. Rev. Lett. **79**, 4760 (1997).

[26] M.L. Mangano, Nucl. Phys. B **405**, 536 (1993).

[27] CDF Collaboration, F. Abe *et al.*, Phys. Rev. D **47**, 4857 (1993).

[28] Lynne H. Orr, T. Stelzer, and W.J. Stirling, Phys. Rev. D **56**, 446 (1997).

TABLE I. Data Sets

Name	Cuts	Events	Background
Standard 3-jet	3 Jets $E_T > 15$ GeV	322	80% ± 4%

	$\mid \eta \mid < 2.$		
SVX b-tagged	3 Jets $E_T > 15$ GeV	34	$25\% \pm 5\%$
	$\mid \eta \mid < 2.$		
	≥ 1 Jet tagged in SVX		

TABLE II. Kinematic Energy Variables

Variable	Definition
P_T(lepton)	The transverse momentum of the highest P_T charged lepton in the event.
$\not\!\!E_T$	The missing transverse energy in the event. It is corrected for μ's above 10 GeV and includes the jet energy correction for all jets with observed $E_T \geq 10$ GeV. Unclustered energy is scaled by a factor of 1.6.
$P_T(1)$	The corrected transverse momentum for the highest E_T jet in the event.
H	The scalar sum of the corrected missing transverse energy, the transverse momentum of the charged lepton, and the transverse momentum of jets with $\mid \eta \mid < 2.4$ and observed $E_T > 8$ GeV.
Mass(W+ 4 jets)	The invariant mass of the W that decays leptonically plus the 4 highest E_T jets. The minimum $\mid P_z \mid$ solution for the neutrino is chosen. If there is no solution with the W mass less than 82 GeV, the magnitude of the neutrino P_T is reduced until a W mass solution of 82 GeV is obtained. This variable is a good approximation to the mass of the $t\bar{t}$ system and is sensitive to longitudinal momentum.
Min Mass(jj)	The minimum di-jet mass.
ΣP_T(jet)	The sum of the transverse momenta of jets with $\mid \eta \mid < 2.4$ and observed $E_T > 8$ GeV.

TABLE III. Kinematic Angular Variables

Variable	Definition
Circularity	The circularity axis of an event is defined in the transverse plane, using the direction along which the sum of the squares of the projected transverse momentum is minimal. This sum when properly normalized is called the circularity. The circularity is also known as the transverse sphericity.
Aplanarity	The aplanarity is calculated using the 3-momenta of the leptonic W (using the minimum $\|P_z\|$ solution for the neutrino) and of the 5 highest E_T jets with uncorrected $E_T > 8$ GeV and $\|\eta\| < 2.4$. The plane with the highest ΣP^2 is determined and the aplanarity is defined as: $1.5 \times \Sigma P^2(\mathrm{out-of-the-plane})/\Sigma P^2(\mathrm{total})$
$\Delta R_{JJ}(\mathrm{min})$	The minimum separation in η-ϕ space between jets.
$\Delta R_{JJ}^{\mathrm{min}} P_T^{\mathrm{min}}/P_T(\mathrm{lepton})$	This is $\Delta R_{JJ}(\mathrm{min})$ times the P_T of the lowest P_T jet in the jet pair determining $\Delta R_{JJ}(\mathrm{min})$ divided by $P_T(\mathrm{lepton})$.
$\Sigma P_Z/\Sigma P_T$	The sum of the $\|P_Z\|$ for the leptonic W and first 4 jets divided by the sum of the P_T of the same objects. The minimum $\|P_Z\|$ neutrino solution is used.
$\cos(\theta^\star)_{\mathrm{max}}$	The maximum $\cos(\theta^\star)$ of the 3 highest E_T jets when transformed to the center of mass of the leptonic W and 4 highest E_T jets. The angle $\theta^\star$ is defined relative to the average direction of the p and $\overline{p}$ in the center of mass.

TABLE IV. The simulated mean of a kinematic variable for $t\bar{t}$ events was determined for different top masses. This table show the result of a linear fit to these means evaluated at a top mass of 175 GeV/c^2 for the three Monte Carlo programs. The units for the momentum variables are GeV/c.

Variable	HERWIG	PYTHIA	ISAJET
P_T(electron)	54.2 ± 0.2	55.0 ± 0.2	55.3 ± 0.3
P_T(muon)	57.8 ± 0.2	59.1 ± 0.3	58.4 ± 0.4
$\not\!\!E_T$	65.7 ± 0.2	65.7 ± 0.2	69.1 ± 0.3
$P_T(1)$	97.9 ± 0.2	99.0 ± 0.2	98.2 ± 0.3
$P_T(2)$	67.2 ± 0.1	67.8 ± 0.1	66.5 ± 0.2
$P_T(3)$	46.4 ± 0.1	46.7 ± 0.1	46.1 ± 0.2
H	365.8 ± 0.4	368.2 ± 0.5	373.5 ± 0.9
$P_T(3)$ + $P_T(4)$	71.2 ± 0.1	71.2 ± 0.2	71.9 ± 0.3
Mass(W + 4 jets)	433.6 ± 0.5	434.5 ± 0.6	428.4 ± 0.9
$\eta_{\max}$	1.088 ± 0.002	1.085 ± 0.003	1.043 ± 0.004
Circularity	0.386 ± 0.002	0.384 ± 0.002	0.378 ± 0.002
Aplanarity	0.0957 ± 0.0004	0.0949 ± 0.0003	0.0963 ± 0.0006

TABLE V. The simulated rms of a kinematic variable for $t\bar{t}$ events was determined for diffferent top masses. This table shows the result of a linear fit to these rms's evaluated at a top mass of 175 GeV/c^2 for the three Monte Carlo programs. The units for the momentum variables are GeV/c.

Variable	HERWIG	PYTHIA	ISAJET
P_T(electron)	28.1 ± 0.2	28.1 ± 0.2	28.7 ± 0.2
P_T(muon)	31.7 ± 0.2	32.7 ± 0.3	32.0 ± 0.2
$\not\!\!E_T$	35.9 ± 0.2	36.6 ± 0.2	37.9 ± 0.2
$P_T(1)$	34.7 ± 0.2	35.8 ± 0.2	36.8 ± 0.2
$P_T(2)$	24.4 ± 0.1	25.1 ± 0.1	25.5 ± 0.1
$P_T(3)$	16.4 ± 0.1	16.7 ± 0.1	16.9 ± 0.1
H	90.4 ± 0.4	94.0 ± 0.5	97.5 ± 0.5
$P_T(3)$ + $P_T(4)$	26.9 ± 0.1	27.2 ± 0.2	28.1 ± 0.1
Mass(W + 4 jets)	101.0 ± 0.5	102.8 ± 0.6	104.9 ± 0.5
$\eta_{\max}$	0.450 ± 0.002	0.451 ± 0.003	0.448 ± 0.002
Circularity	0.224 ± 0.002	0.222 ± 0.002	0.222 ± 0.002
Aplanarity	0.0698 ± 0.0004	0.0687 ± 0.0004	0.0696 ± 0.004

TABLE VI. This table is a comparison of the simulated means for the Standard 3-jet and SVX b-tagged data sets. The means for both samples using HERWIG $t\bar{t}$ events evaluated at a top mass of 175 GeV/c^2 are shown. The units for the momentum variables are GeV/c.

Variable	HERWIG	HERWIG(b-tag)
P_T(electron)	54.2 ± 0.2	54.3 ± 0.3
P_T(muon)	57.8 ± 0.2	57.8 ± 0.3
$\not\!\!E_T$	65.7 ± 0.2	65.5 ± 0.3
$P_T(1)$	97.9 ± 0.2	99.6 ± 0.2
$P_T(2)$	67.2 ± 0.1	69.3 ± 0.2
$P_T(3)$	46.4 ± 0.1	47.8 ± 0.1
H = P_T(lepton) + $\not\!\!E_T$ + ΣP_T(jet)	365.8 ± 0.4	371.6 ± 0.6
$P_T(3)$ + $P_T(4)$	71.2 ± 0.1	73.3 ± 0.2
Mass(W + 4 jets)	433.6 ± 0.5	435.7 ± 0.7
$\eta_{\max}$	1.088 ± 0.002	1.040 ± 0.003
Circularity	0.386 ± 0.002	0.394 ± 0.002
Aplanarity	0.0957 ± 0.0004	0.0986 ± 0.0005

TABLE VII. rms/slope for the energy variables using fits to HERWIG $t\bar{t}$ events evaluated at a top mass of 175 GeV/c^2.

$$\Delta M_{top} \approx \frac{1}{\sqrt{N}} \left(\frac{rms}{slope}\right)$$

Variable	$\frac{rms}{slope}$ (GeV/c^2)
P_T(electron)	184. ± 14.
P_T(muon)	187. ± 18.
$\not\!\!E_T$	167. ± 9.
$P_T(1)$	66. ± 1.
$P_T(2)$	72. ± 1.
$P_T(3)$	87. ± 2.
$H(\Sigma\ P_T)$	57. ± 1.
$P_T(2) + P_T(3)$	68. ± 1.
$P_T(3) + P_T(4)$	91. ± 2.
Mass(W + 4 jets)	57. ± 1.

TABLE VIII. The table compares different $t\bar{t}$ generators with PYTHIA using the KS (Kolmogorov-Smirnov) probabilities for several kinematic variables.

KS Test Probabilities with PYTHIA				
Variable	HERWIG	ISAJET	PYTHIA (no ISR)	PYTHIA (no FSR)
P_T(lepton)	0.808	0.052	0.629	0.115
$\not\!\!E_T$	0.141	0.023	0.054	0.771
P_T(W leptonic)	0.048	0.267	0.031	0.147
P_T(1)	0.013	0.690	0.022	0.000
P_T(2)	0.872	0.033	0.281	0.000
P_T(3)	0.538	0.150	0.014	0.000
Min Mass(jj)	0.933	0.034	0.313	0.000
H	0.086	0.332	0.000	0.000
$P_T(3) + P_T(4)$	0.343	0.560	0.000	0.000
Mass(W + 4 jets)	0.996	0.116	0.000	0.000
$\Sigma P_Z/\Sigma P_T$	0.756	0.002	0.003	0.180
$\cos(\theta^\star)_{\max}$	0.676	0.056	0.208	0.300
Circularity	0.037	0.103	0.934	0.006
Aplanarity	0.193	0.940	0.193	0.008
$\Delta R_{JJ}^{min} * P_T^{min}/P_T$(lepton)	0.918	0.094	0.802	0.000
Average	0.49	0.23	0.23	0.10

TABLE IX. The table shows the predictions for the different generators of the fraction of the SVX b-tagged sample with both a fourth and fifth jet with observed $E_T > 8$ GeV and $|\eta| < 2.4$. The final column shows the expected number of events for the observed SVX b-tagged sample size of 34.

Monte Carlo Predictions for Fraction of Events with 5 Jets			
Monte Carlo	$t\bar{t}$	($t\bar{t}$ + VECBOS)	Expected number of events
ISAJET	0.445	0.370	12.6
HERWIG	0.359	0.305	10.4
PYTHIA	0.332	0.285	9.7
PYTHIA (no ISR)	0.196	0.183	6.2
PYTHIA (no FSR)	0.175	0.167	5.7
PYTHIA (no FSR + no ISR)	0.003	0.038	1.3

TABLE X. The mean of the data and its error are given for several variables in the third column. The means for the QCD background (VECBOS) and $t\bar{t}$ (HERWIG with a top mass of 175 GeV/c^2) are shown in the second and fourth columns. Momentum variables are in units of GeV/c.

Luminosity = 109 pb^{-1}

Means for 322 Standard 3-jet sample

Variable	VECBOS	DATA	TOP 175
P_T(electron)	49.9	50.7 ± 2.0	54.4
$\not\!\!E_T$	52.8	54.4 ± 1.8	65.4
$P_T(W \to e\ \nu)$	73.6	74.2 ± 2.6	91.6
$P_T(1)$	75.0	76.1 ± 2.1	98.0
$P_T(2)$	47.8	51.9 ± 1.3	67.3
$P_T(3)$	33.2	36.2 ± 0.7	46.4
Min Mass(jj)	46.1	50.1 ± 1.5	59.5
ΣP_T(jet)	168.1	180.7 ± 4.0	243.2
H = P_T(lepton) + $\not\!\!E_T$ + ΣP_T(jet)	273.9	289.0 ± 5.2	365.9
$P_T(2) + P_T(3)$	80.9	88.1 ± 1.8	113.3
$P_T(3) + P_T(4)$	44.4	49.3 ± 1.3	71.2
Mass(W + 4 jets)	365.0	372.1 ± 6.4	433.9
$\Sigma P_Z/\Sigma P_T$	0.948	0.927 ± 0.024	0.732
$\cos(\theta^\star)_{max}$	0.752	0.728 ± 0.010	0.673
Circularity	0.327	0.337 ± 0.013	0.391
Aplanarity	0.058	0.068 ± 0.003	0.095
$\Delta R_{JJ}^{min} P_T^{min}/P_T$(lepton)	0.606	0.658 ± 0.028	0.743

TABLE XI. The mean of the data and its error are given for several variables in the third column. The means for the QCD background (VECBOS) and $t\bar{t}$ (HERWIG with a top mass of 175 GeV/c^2) are shown in the second and fourth columns. Momentum variables are in units of GeV/c.

Luminosity = 109 pb^{-1}

Means for 34 SVX b-tagged sample

Variable	VECBOS	DATA	TOP 175
P_T(electron)	51.0	55.0 ± 6.9	54.2
$\not\!\!E_T$	53.9	69.7 ± 6.0	64.9
$P_T(W \to e\,\nu)$	76.4	93.2 ± 8.3	90.6
$P_T(1)$	76.6	89.0 ± 6.2	99.9
$P_T(2)$	49.6	65.1 ± 4.4	69.7
$P_T(3)$	34.3	44.5 ± 2.9	48.0
P_T^{b-jet}(jet)	53.3	74.0 ± 6.0	80.0
Min Mass(jj)	45.6	59.1 ± 4.5	60.6
H = P_T(lepton) + $\not\!\!E_T$ + ΣP_T(jet)	281.4	349.1 ± 16.7	371.5
$P_T(2) + P_T(3)$	83.8	109.6 ± 6.4	117.0
$P_T(3) + P_T(4)$	46.6	65.0 ± 4.9	73.6
Mass(W + 4 jets)	365.8	413.8 ± 18.5	437.5
$\Sigma P_Z/\Sigma P_T$	0.869	0.676 ± 0.059	0.707
$\cos(\theta^\star)_{max}$	0.731	0.687 ± 0.032	0.660
Circularity	0.325	0.381 ± 0.039	0.395
Aplanarity	0.062	0.101 ± 0.012	0.099
$\Delta R_{JJ}^{min} P_T^{min}/P_T$(lepton)	0.589	0.698 ± 0.097	0.754

TABLE XII. The means and their principal systematic uncertainties are shown for the QCD background (VECBOS) and $t\bar{t}$ (HERWIG with a top mass of 175 GeV/c^2). The uncertainties shown for VECBOS are due to the Q^2 scale and jet energy scale systematics. The uncertainties for $t\bar{t}$ are due to uncertainty in the top mass and the jet energy scale systematics. Momentum variables are in units of GeV/c.

Means for 322 Standard 3-jet sample		
Variable	VECBOS $\pm Q^2$scale$\pm$Escale	$t\bar{t}$ $\pm$mass$\pm$Escale
P_T(electron)	$49.9 \pm 0.0 \pm 0.3$	$54.4 \pm 0.8 \mp 0.1$
$\not\!\!E_T$	$52.8 \mp 0.0 \mp 1.2$	$65.4 \pm 1.2 \mp 0.4$
$P_T(W \to e\ \nu)$	$73.6 \mp 0.8 \mp 2.1$	$91.6 \pm 2.4 \mp 0.8$
$P_T(1)$	$75.0 \pm 1.1 \pm 0.5$	$98.0 \pm 2.4 \pm 3.1$
$P_T(2)$	$47.8 \pm 1.2 \pm 0.3$	$67.3 \pm 1.6 \pm 2.0$
$P_T(3)$	$33.2 \pm 0.5 \pm 0.2$	$46.4 \pm 1.0 \pm 1.3$
Min Mass(jj)	$46.1 \pm 0.6 \mp 0.5$	$59.5 \pm 1.2 \pm 1.3$
ΣP_T(jet)	$168.1 \pm 3.2 \pm 1.7$	$243.2 \pm 5.8 \pm 8.4$
H = P_T(lepton) + $\not\!\!E_T$ + ΣP_T(jet)	$273.9 \pm 2.8 \pm 0.2$	$365.9 \pm 7.8 \pm 7.9$
$P_T(2) + P_T(3)$	$80.9 \pm 1.6 \pm 0.4$	$113.3 \pm 2.5 \pm 3.2$
$P_T(3) + P_T(4)$	$44.4 \pm 0.7 \pm 0.8$	$71.2 \pm 1.5 \pm 2.5$
Mass(W + 4 jets)	$365.0 \pm 0.4 \pm 1.8$	$433.9 \pm 8.3 \pm 9.7$
$\Sigma P_Z/\Sigma P_T$	$0.948 \mp 0.001 \pm 0.014$	$0.732 \mp 0.006 \pm 0.006$
$\cos(\theta^\star)_{max}$	$0.752 \mp 0.004 \pm 0.003$	$0.673 \mp 0.000 \pm 0.003$
Circularity	$0.327 \mp 0.001 \pm 0.002$	$0.391 \mp 0.002 \pm 0.000$
Aplanarity	$0.058 \pm 0.000 \pm 0.000$	$0.095 \pm 0.000 \pm 0.001$
$\Delta R_{JJ}^{min} P_T^{min}/P_T$(lepton)	$0.606 \pm 0.002 \pm 0.004$	$0.743 \pm 0.004 \pm 0.016$

TABLE XIII. The means and their principal systematic uncertainties are shown for the QCD background (VECBOS) and $t\bar{t}$ (HERWIG with a top mass of 175 GeV/c^2). The uncertainties shown for VECBOS are due to the Q^2 scale and jet energy scale systematics. The uncertainties for $t\bar{t}$ are due to uncertainty in the top mass and the jet energy scale systematics. Momentum variables are in units of GeV/c.

Means for 34 SVX b-tagged sample		
Variable	VECBOS $\pm Q^2$scale$\pm$Escale	$t\bar{t}$ $\pm$mass$\pm$Escale
P_T(electron)	$51.0 \mp 0.2 \pm 0.1$	$54.2 \pm 0.8 \pm 0.0$
$\not\!\!E_T$	$53.9 \mp 0.9 \mp 1.0$	$64.9 \pm 1.4 \mp 0.4$
$P_T(W \to e\ \nu)$	$76.4 \mp 1.9 \pm 1.4$	$90.6 \pm 3.0 \mp 0.7$
$P_T(1)$	$76.6 \pm 1.2 \pm 0.8$	$99.9 \pm 2.2 \pm 3.3$
$P_T(2)$	$49.6 \pm 1.1 \pm 0.6$	$69.7 \pm 1.2 \pm 2.1$
$P_T(3)$	$34.3 \pm 0.6 \pm 0.3$	$48.0 \pm 0.7 \pm 1.4$
P_T^{b-tag}(jet)	$53.3 \pm 0.9 \pm 1.7$	$80.0 \pm 2.3 \pm 2.7$
Min Mass(jj)	$45.6 \pm 1.1 \mp 0.4$	$60.6 \pm 0.9 \pm 1.6$
H = P_T(lepton) + $\not\!\!E_T$ + ΣP_T(jet)	$281.4 \pm 2.1 \pm 1.0$	$371.5 \pm 7.4 \pm 8.3$
$P_T(2) + P_T(3)$	$83.8 \pm 1.7 \pm 0.8$	$117.0 \pm 1.7 \pm 3.4$
$P_T(3) + P_T(4)$	$46.6 \pm 0.7 \pm 1.0$	$73.6 \pm 1.0 \pm 2.6$
Mass(W + 4 jets)	$365.8 \pm 1.0 \pm 2.9$	$437.5 \pm 6.3 \pm 10.1$
$\Sigma P_Z/\Sigma P_T$	$0.869 \pm 0.009 \pm 0.008$	$0.707 \mp .011 \pm 0.005$
$\cos(\theta^\star)_{max}$	$0.731 \mp 0.002 \pm 0.004$	$0.660 \mp 0.001 \pm 0.003$
Circularity	$0.325 \mp 0.001 \pm 0.004$	$0.395 \mp 0.003 \pm 0.001$
Aplanarity	$0.062 \pm 0.001 \pm 0.001$	$0.099 \mp 0.000 \pm 0.001$
$\Delta R_{JJ}^{min} P_T^{min}/P_T$(lepton)	$0.589 \pm 0.008 \pm 0.001$	$0.754 \mp 0.006 \pm 0.020$

TABLE XIV. The table gives the χ^2 probabilities and KS (Kolmogorov-Smirnov) probabilities from a comparison of the data to the Monte Carlo predictions as shown in the distribution plots. Columns 2 and 3 are for the 322 event Standard 3-jet sample and columns 4 and 5 are for the 34 event SVX b-tagged sample.

	Top mass for Monte Carlo = 175 GeV/c^2			
Variable	χ^2 (Probability)	KS (Probability)	χ^2 (Probability)	KS (Probability)
	W + 3 Jet	W + 3 Jet	SVX b-tag	SVX b-tag
P_T(lepton)	0.68	0.59	0.99	0.95
$\not\!\!E_T$	0.70	0.93	0.22	0.19
P_T(W leptonic)	0.45	0.72	0.73	0.88
P_T(1)	0.52	0.06	0.37	0.54
P_T(2)	0.40	0.80	0.60	0.69
P_T(3)	0.58	0.97	0.30	0.94
Min Mass(jj)	0.26	0.75	0.08	0.56
H	0.12	0.10	0.99	1.00
$P_T(3) + P_T(4)$	0.56	0.40	0.59	0.94
Mass(W + 4 jets)	0.02	0.04	0.95	0.97
$\Sigma P_Z/\Sigma P_T$	0.12	0.12	0.47	0.49
$\cos(\theta^*)_{max}$	0.59	0.37	0.37	0.55
Circularity	0.32	0.48	0.66	0.93
Aplanarity	0.13	0.68	0.29	0.58
$\Delta R_{JJ}^{min} * P_T^{min}/P_T$(lepton)	0.76	0.50	0.86	0.98
Average	0.41	0.50	0.56	0.75

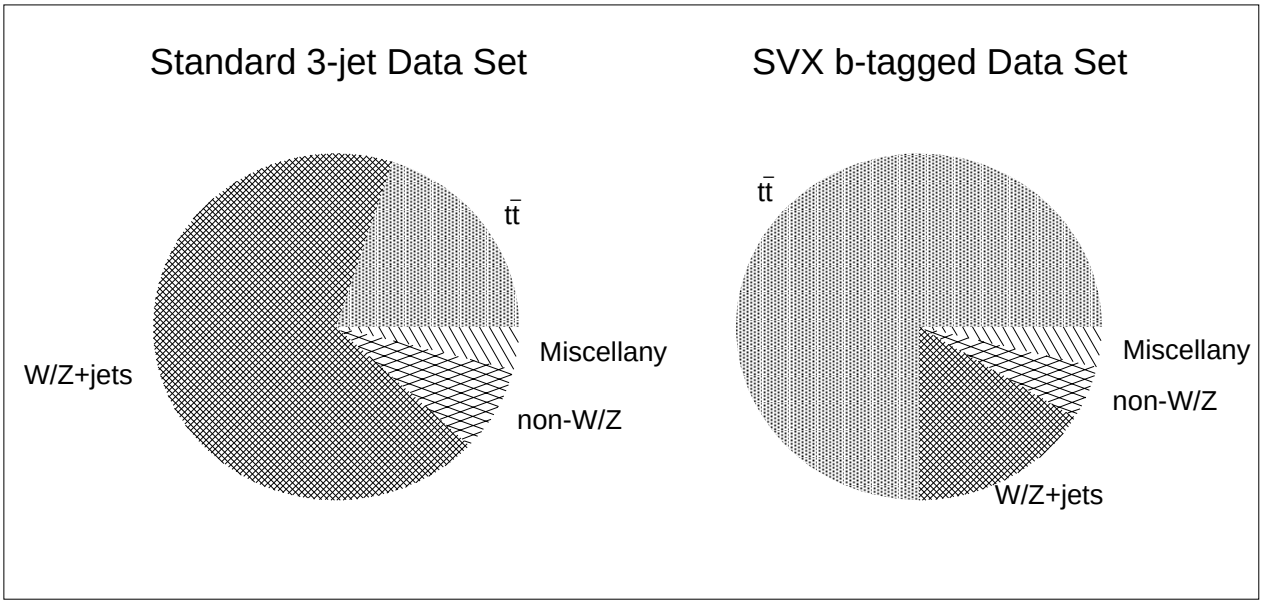

FIG. 1. The figure shows the fractions of $t\bar{t}$ signal and backgrounds for the two data sets. The background categories are QCD W/Z + jets, non-W/Z, and Miscellany.

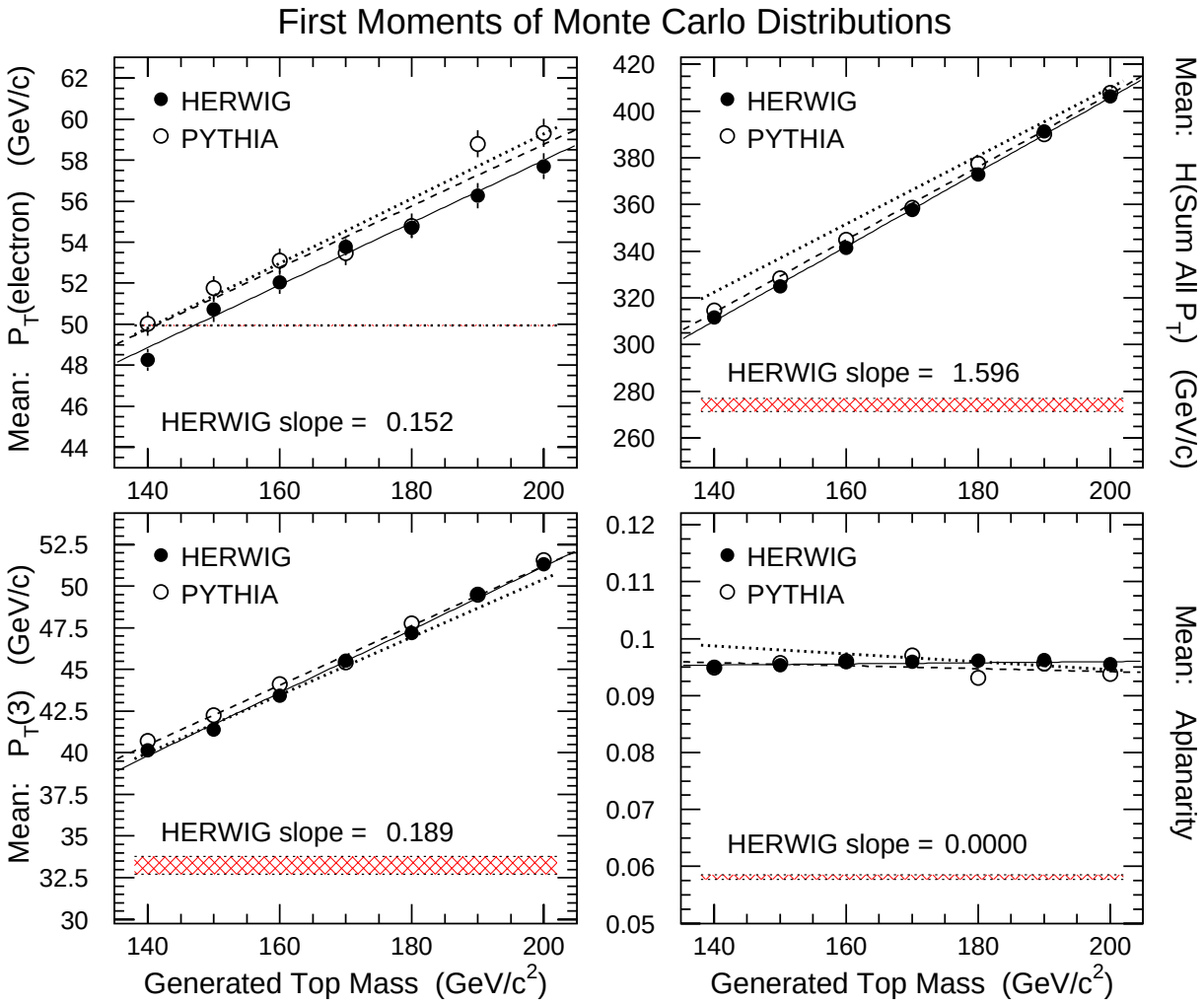

FIG. 2. The means of four variables for simulated $t\bar{t}$ events versus the value of top mass. The solid circles are the values for HERWIG and the open circles for PYTHIA. The solid lines are the result of a linear fit to the points for HERWIG, the dashed lines for PYTHIA, and the dotted lines for ISAJET. The horizontal hatched bands are the predictions for the QCD background (VECBOS); the band widths show the variation between $Q^2 =< \mathrm{P_T} >^2$ and M_W^2.

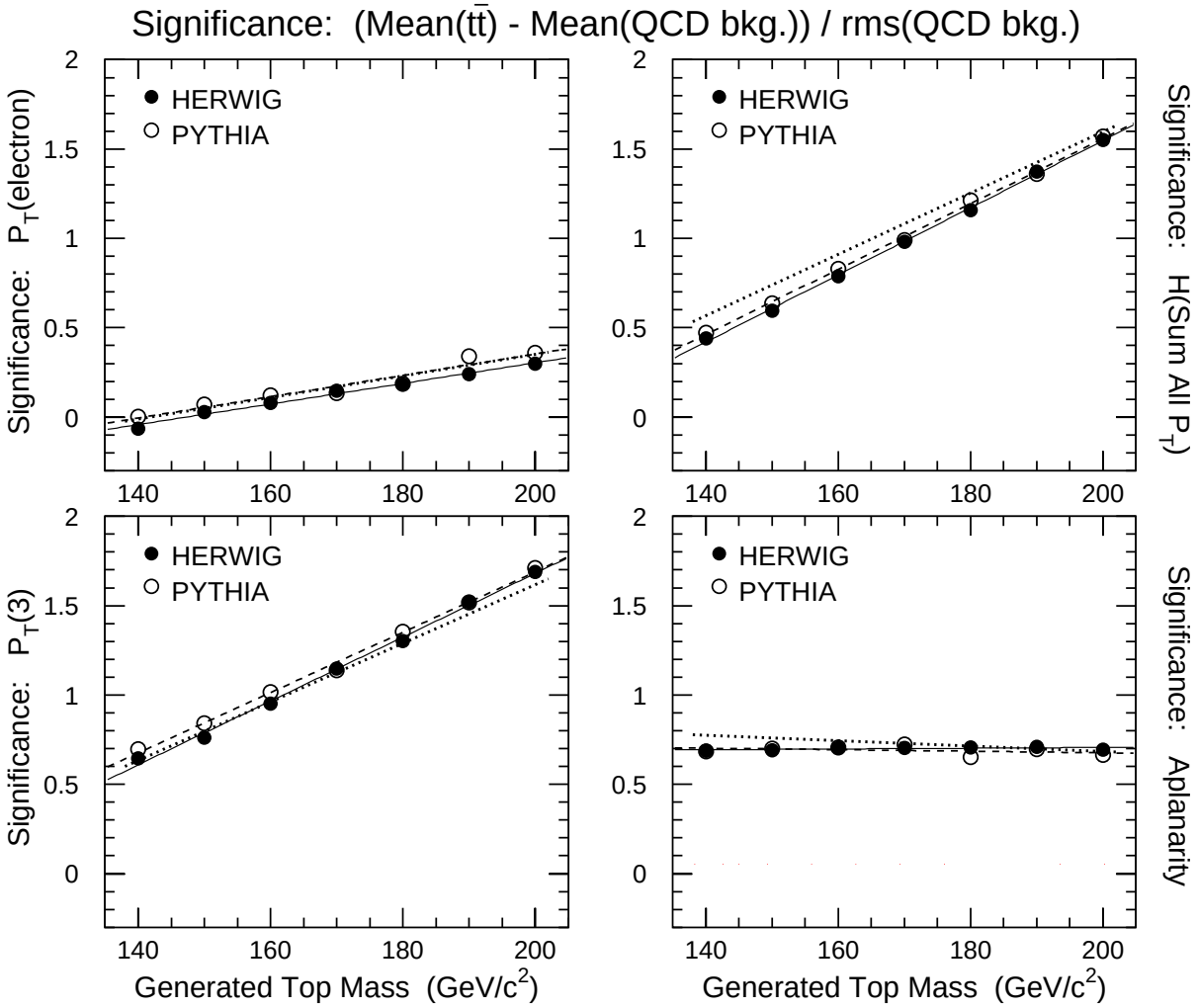

FIG. 3. The Significance of differences between the means for simulated $t\bar{t}$ events and QCD background events (VECBOS) versus the value of top mass. Significance is defined as (Mean($t\bar{t}$) - Mean(QCD background))/rms(QCD background). The solid circles are the values for HERWIG and the open circles for PYTHIA. The solid lines are the result of a linear fit to the points for HERWIG, the dashed lines for PYTHIA, and the dotted lines for ISAJET.

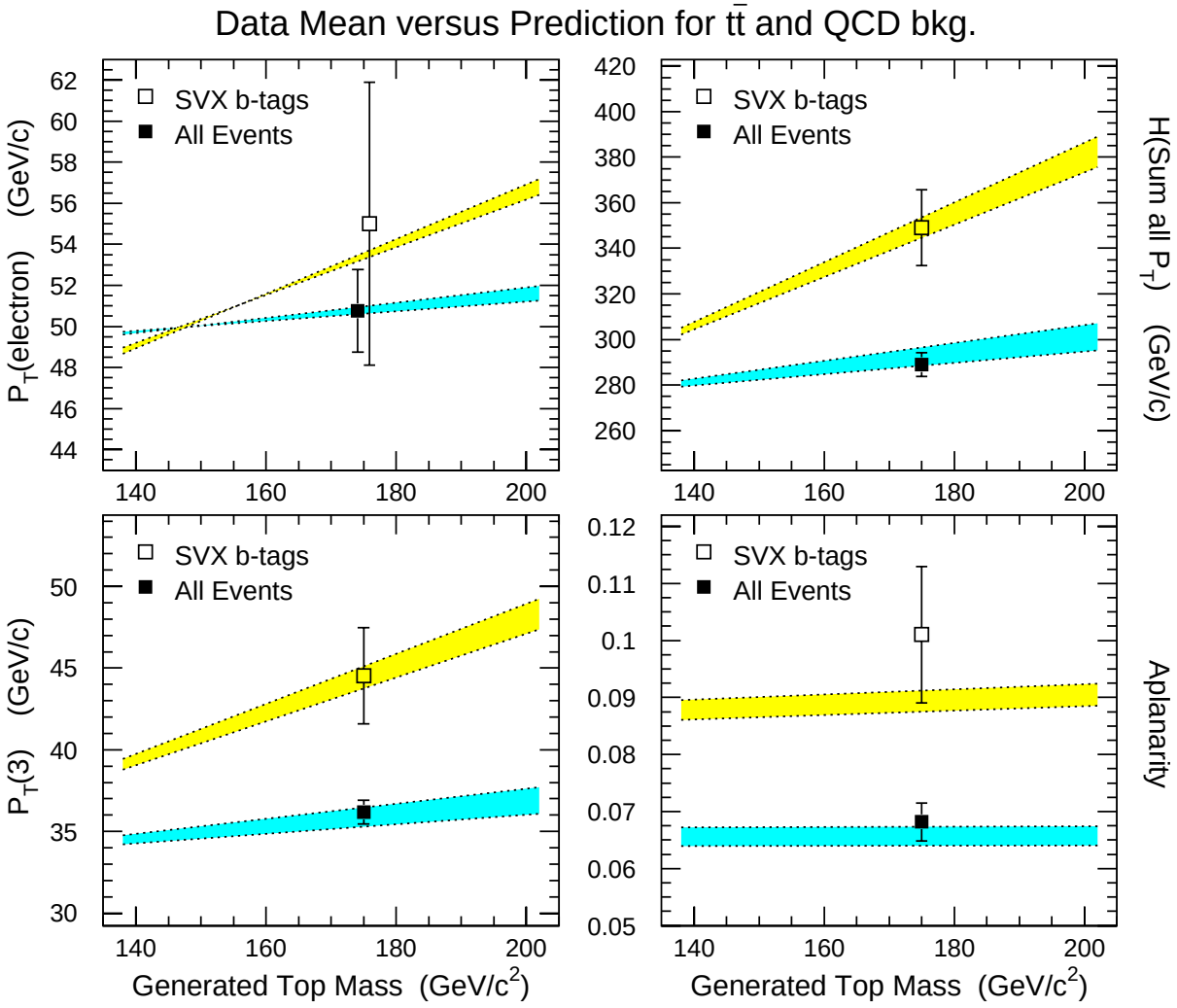

FIG. 4. The prediction for the expected mixture of $t\bar{t}$ production and QCD background versus the value of top mass for four variables. The bands show the predictions, the widths of the bands represent the uncertainty in the $t\bar{t}$ fraction. The data points are plotted with statistical error bars at a top mass of 175 GeV/c^2; the solid squares represent the mean of the Standard 3-jet sample and the open squares the SVX b-tagged sample.

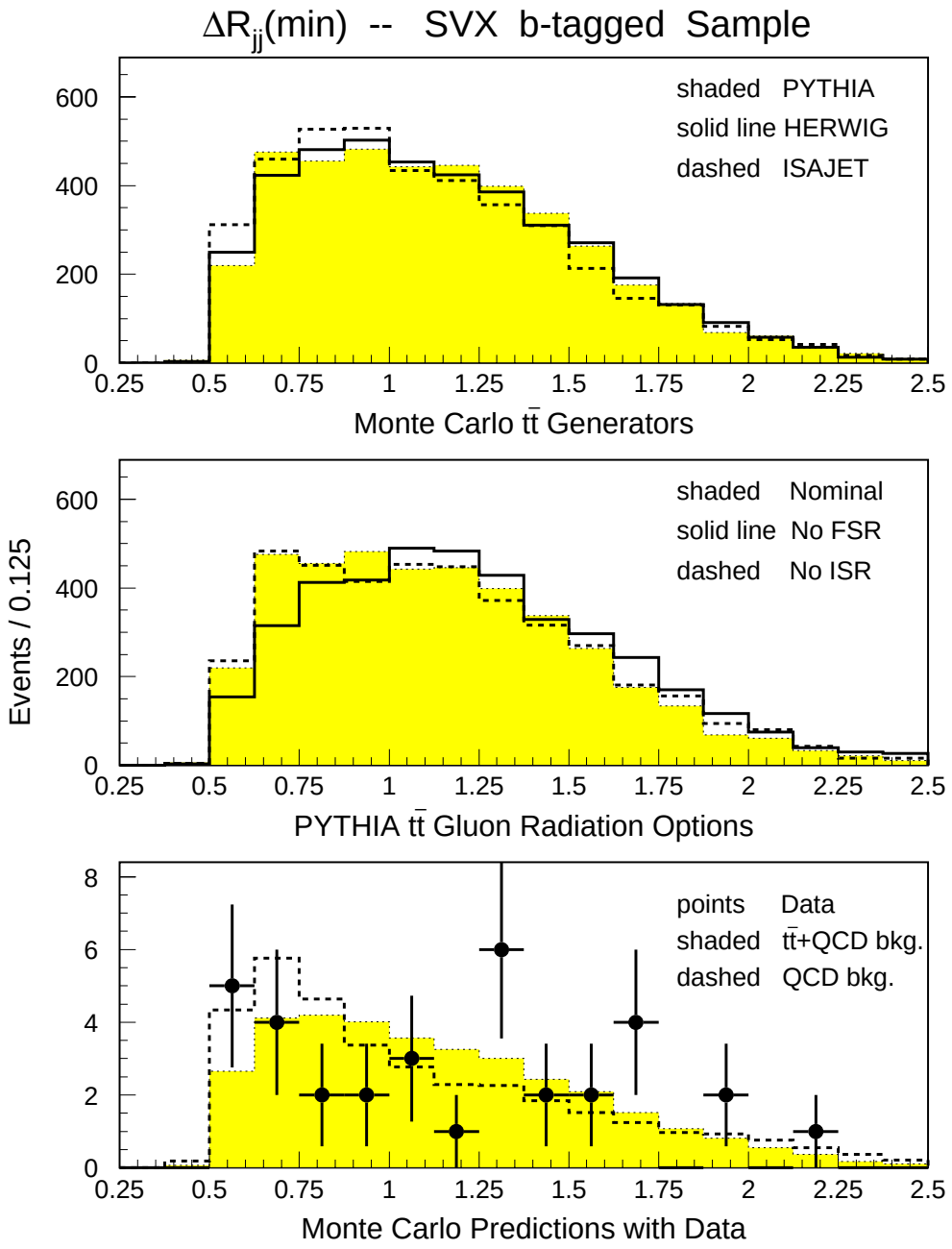

FIG. 5. Distributions of minimum jet-jet separation for gluon radiation studies. The top plot shows the predictions for the three $t\bar{t}$ generators. The middle plot shows the predictions for PYTHIA with different gluon radiation options. The bottom plot compares the data (solid points with error bars) to predictions for the expected mixture of $t\bar{t}$ and QCD background and QCD background alone.

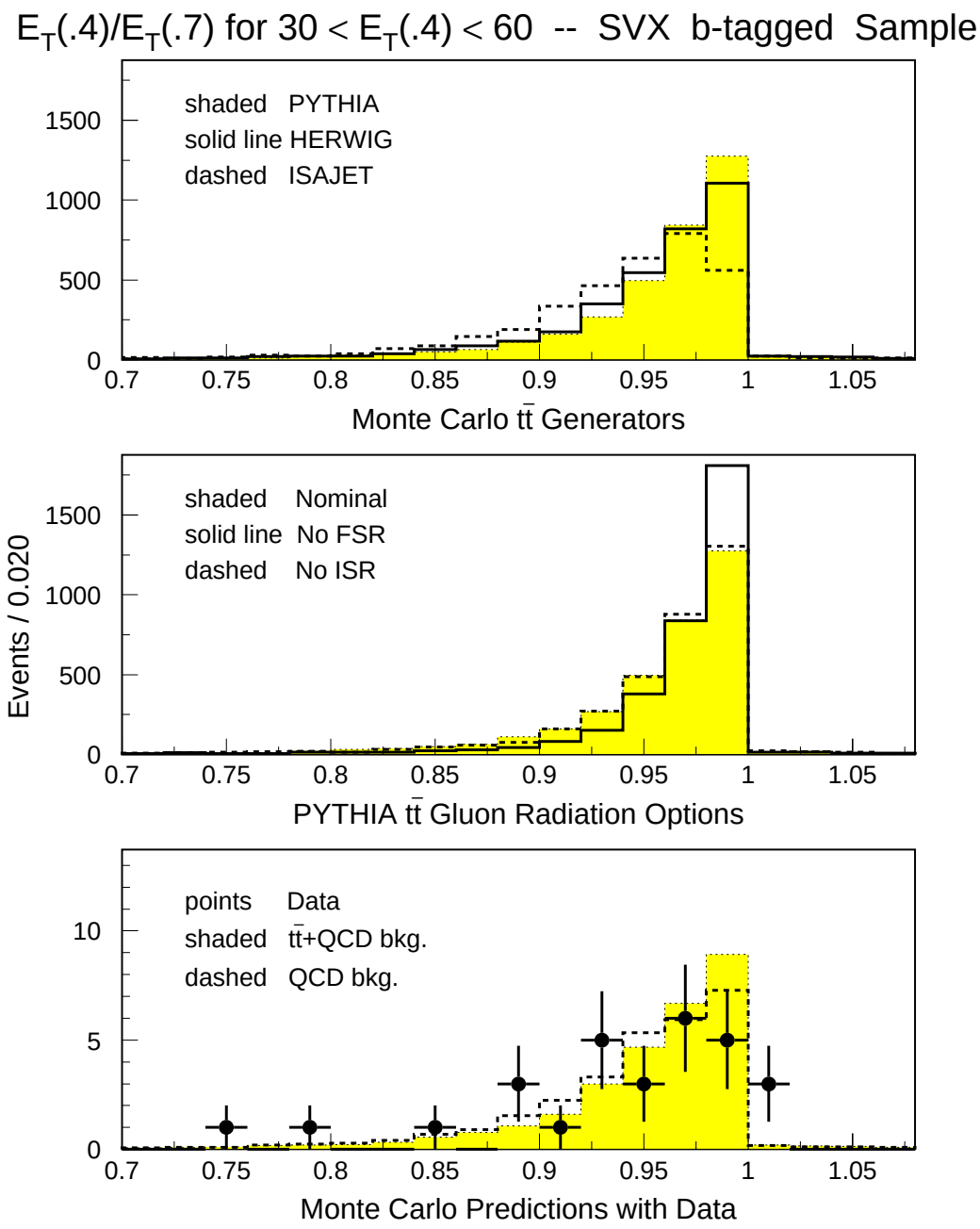

FIG. 6. Distributions of $E_T(0.4)/E_T(0.7)$ for gluon radiation studies. The top plot shows the predictions for the three $t\bar{t}$ generators. The middle plot shows the predictions for PYTHIA with different gluon radiation options. The bottom plot compares the data (solid points with error bars) to predictions for the expected mixture of $t\bar{t}$ and QCD background and QCD background alone.

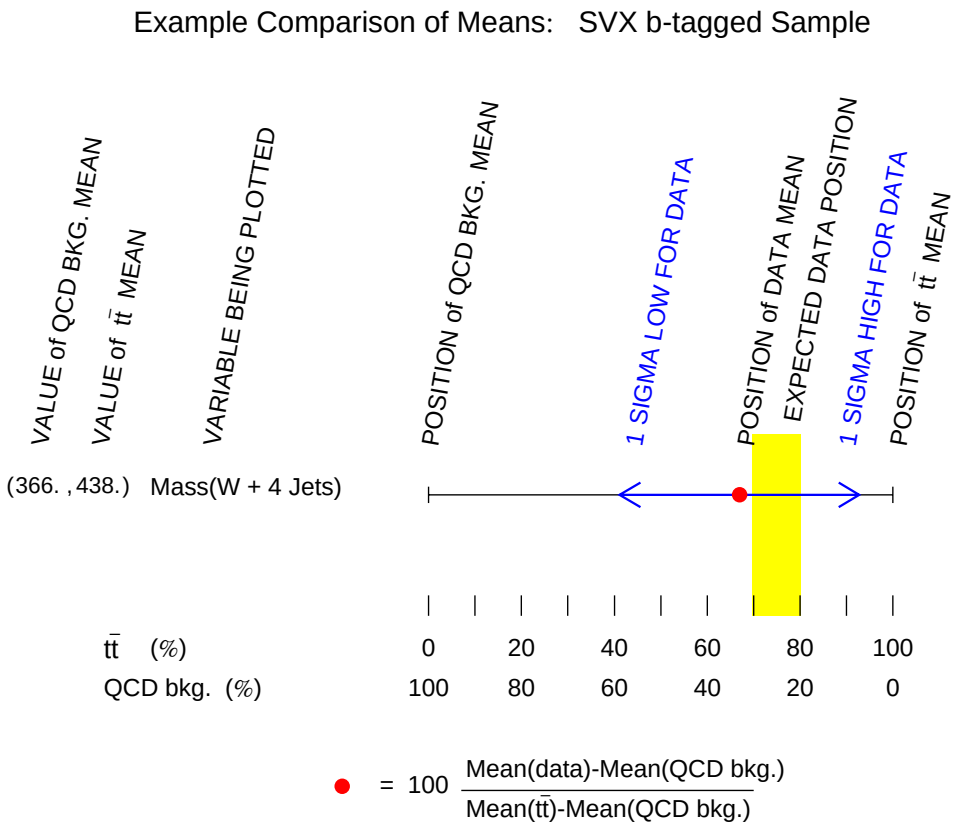

FIG. 7. Example plot for the graphical comparison of the data mean to simulated means. The data and its statistical uncertainity are represented by the solid circle and the arrows. The tick at the left end of the line graphically represents the mean for 100% QCD background (VECBOS) and the tick at the right end of the line the mean for 100% $t\bar{t}$ (HERWIG with a top mass of 175 GeV/c^2).

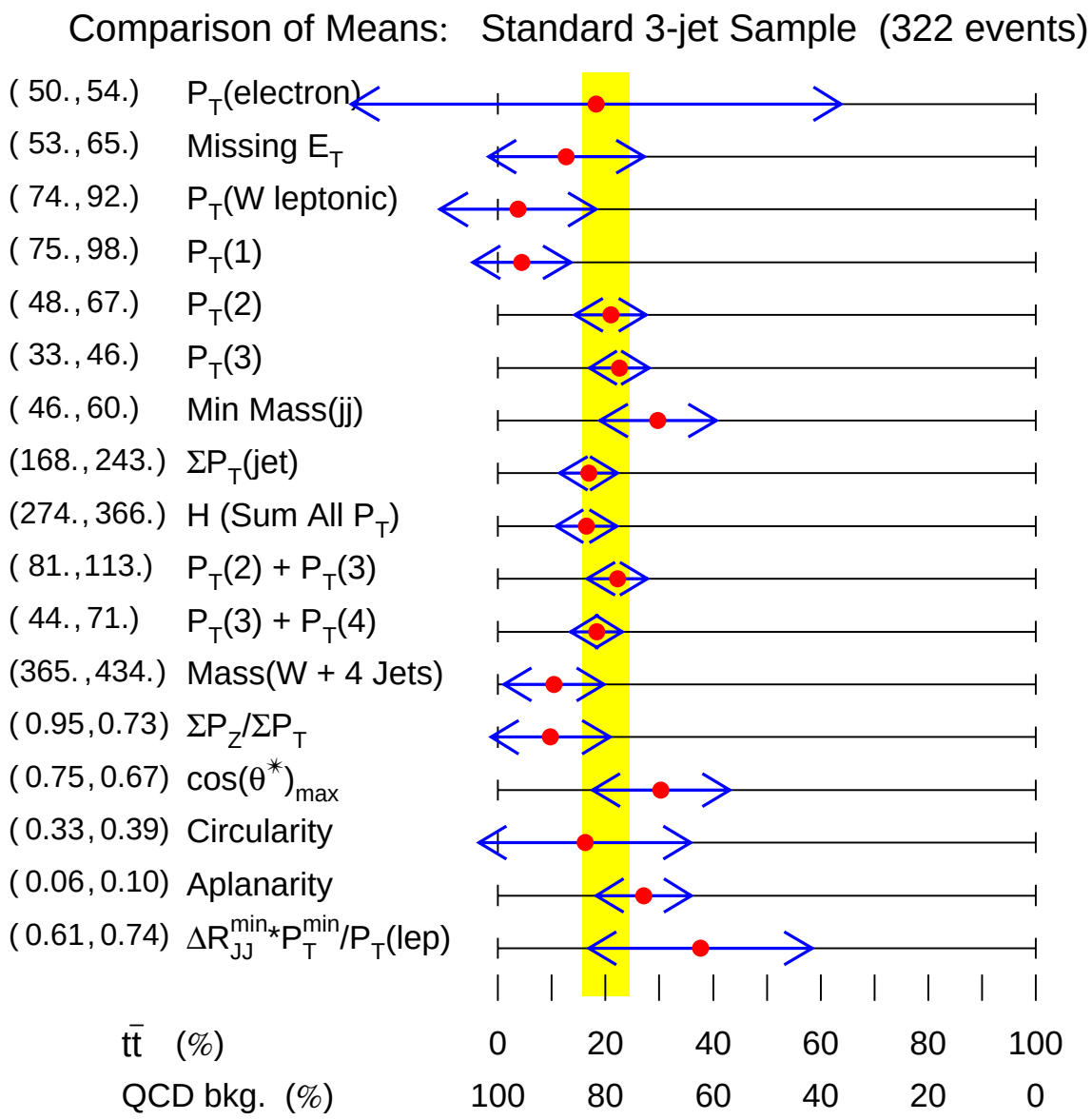

FIG. 8. Comparison of means for the Standard 3-jet sample. The data and its statistical uncertainty are represented by the solid circles and the arrows. The left end of each line graphically represents the mean for 100% QCD background (VECBOS) and the right end of each line the mean for 100% $t\bar{t}$ (HERWIG). The numbers on the far left are the values of the means for QCD background and $t\bar{t}$, respectively.

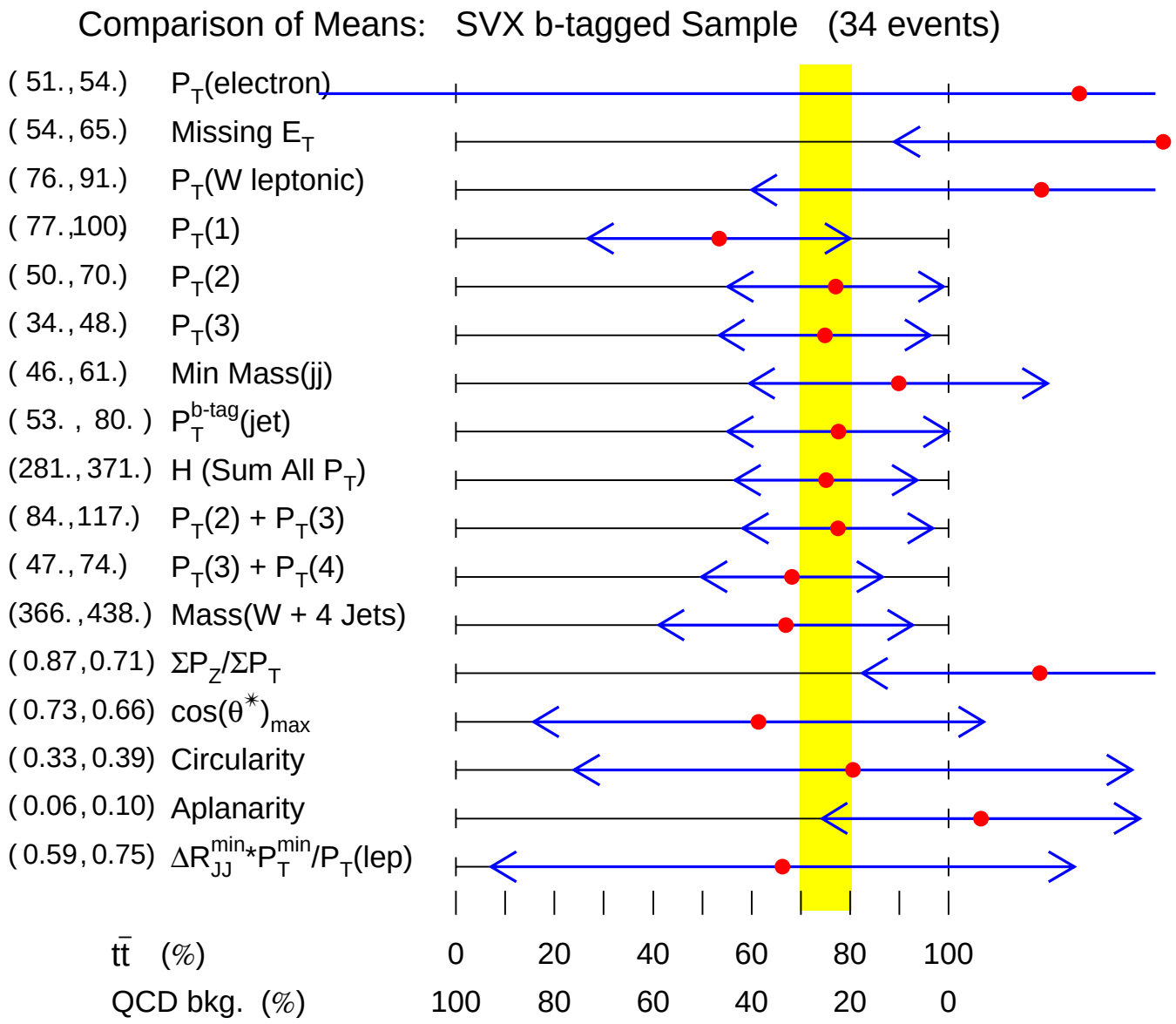

FIG. 9. Comparison of means for the SVX b-tagged data sample. The data and its statistical uncertainty are represented by the solid circles and the arrows. The left end of each line graphically represents the mean for 100% QCD background (VECBOS) and the right end of each line the mean for 100% $t\bar{t}$ (HERWIG). The numbers on the far left are the values of the means for QCD background and $t\bar{t}$, respectively.

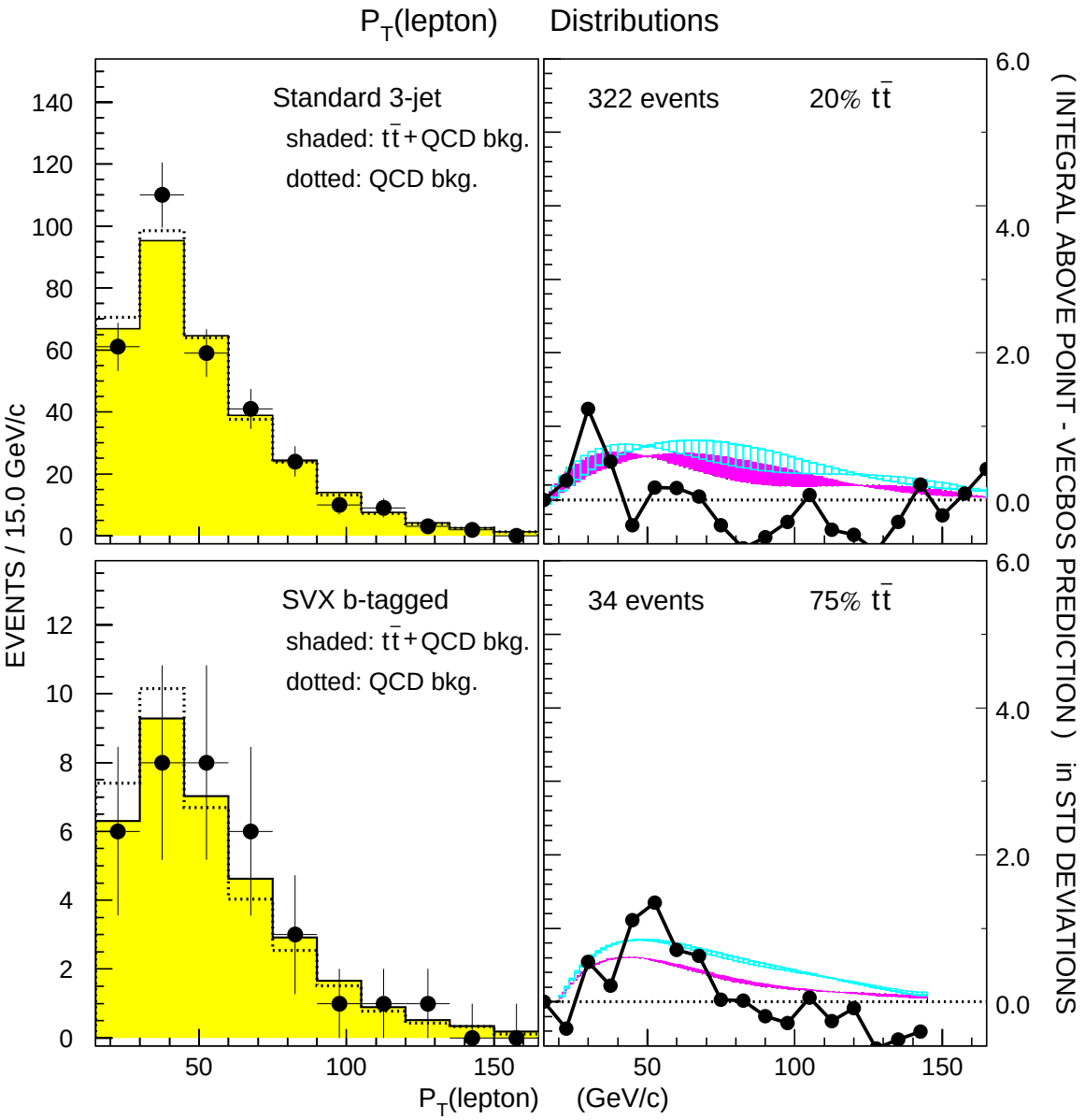

FIG. 10. Comparison of the data with Monte Carlo predictions for P_T(lepton). Differential plots are on the left; the solid points with error bars are the data and the histograms are the Monte Carlo predictions normalized to the data. The integral significance plots are on the right; the data are the solid points. The shaded band is the prediction for the expected mixture of $t\bar{t}$ and QCD background for 175 GeV/c^2 top; the hatched band is the equivalent for 185 GeV/c^2 top. The width of the bands represent the uncertainty in the QCD background due to Q^2 scale variations. A data point one vertical unit from the shaded band corresponds to a one σ deviation.

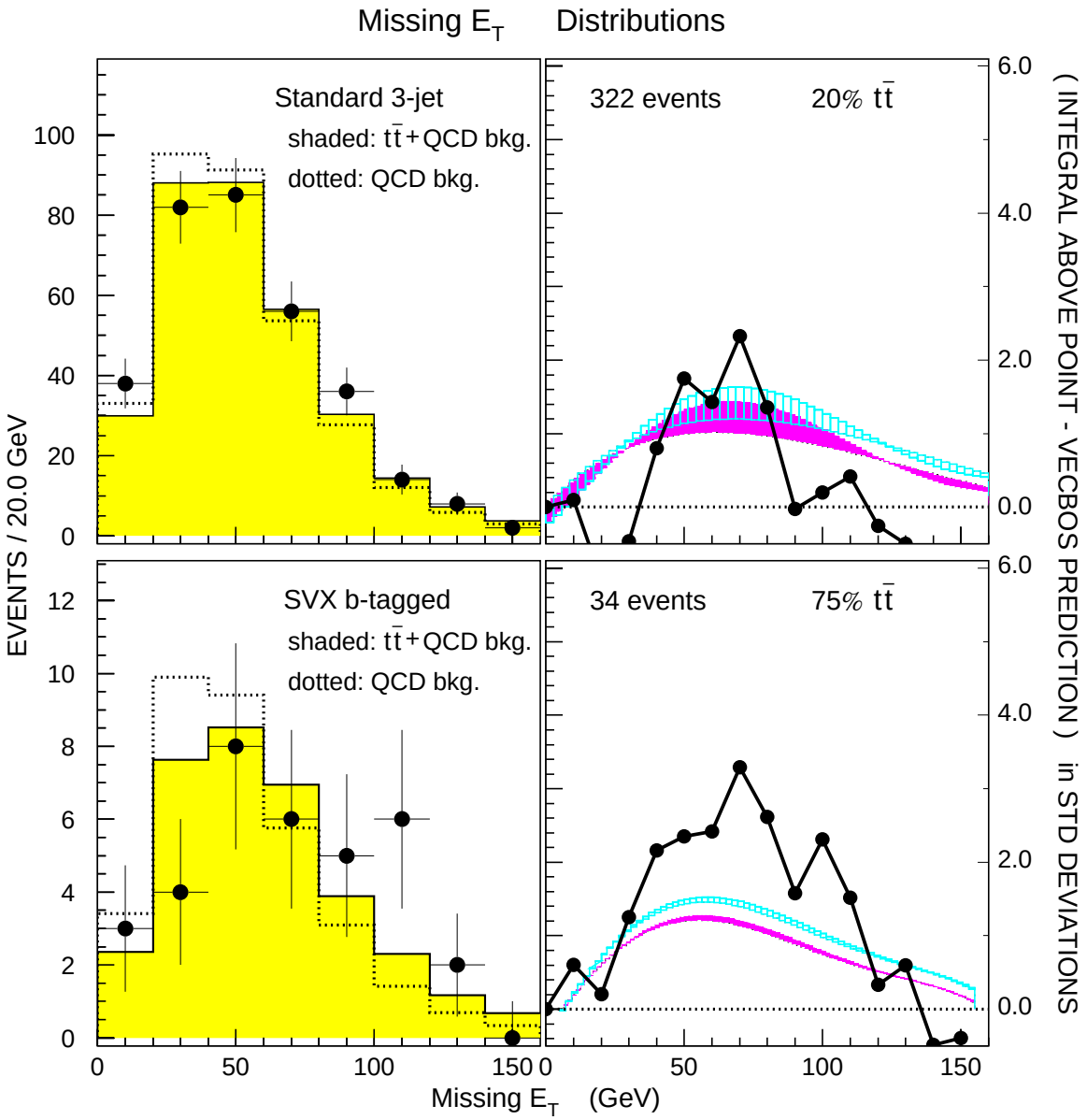

FIG. 11. Comparison of the data with Monte Carlo predictions for Corrected missing E_T. Differential plots are on the left; the solid points with error bars are the data and the histograms are the Monte Carlo predictions normalized to the data. The integral significance plots are on the right; the data are the solid points. The shaded band is the prediction for the expected mixture of $t\bar{t}$ and QCD background for 175 GeV/c^2 top; the hatched band is the equivalent for 185 GeV/c^2 top. The width of the bands represent the uncertainty in the QCD background due to Q^2 scale variations. A data point one vertical unit from the shaded band corresponds to a one σ deviation.

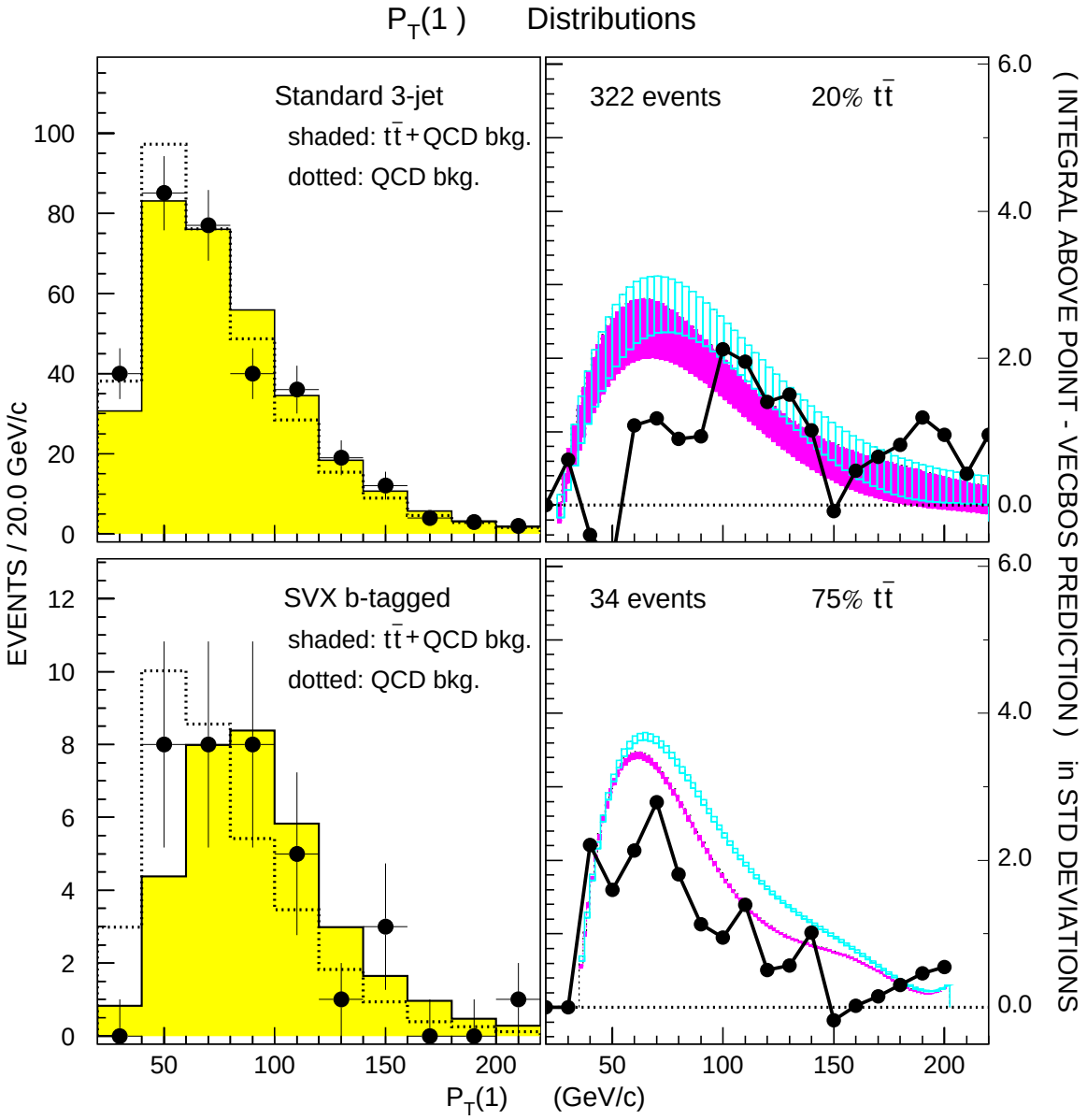

FIG. 12. Comparison of the data with Monte Carlo predictions for $P_T(1)$. Differential plots are on the left; the solid points with error bars are the data and the histograms are the Monte Carlo predictions normalized to the data. The integral significance plots are on the right; the data are the solid points. The shaded band is the prediction for the expected mixture of $t\bar{t}$ and QCD background for 175 GeV/c^2 top; the hatched band is the equivalent for 185 GeV/c^2 top. The width of the bands represent the uncertainty in the QCD background due to Q^2 scale variations. A data point one vertical unit from the shaded band corresponds to a one σ deviation.

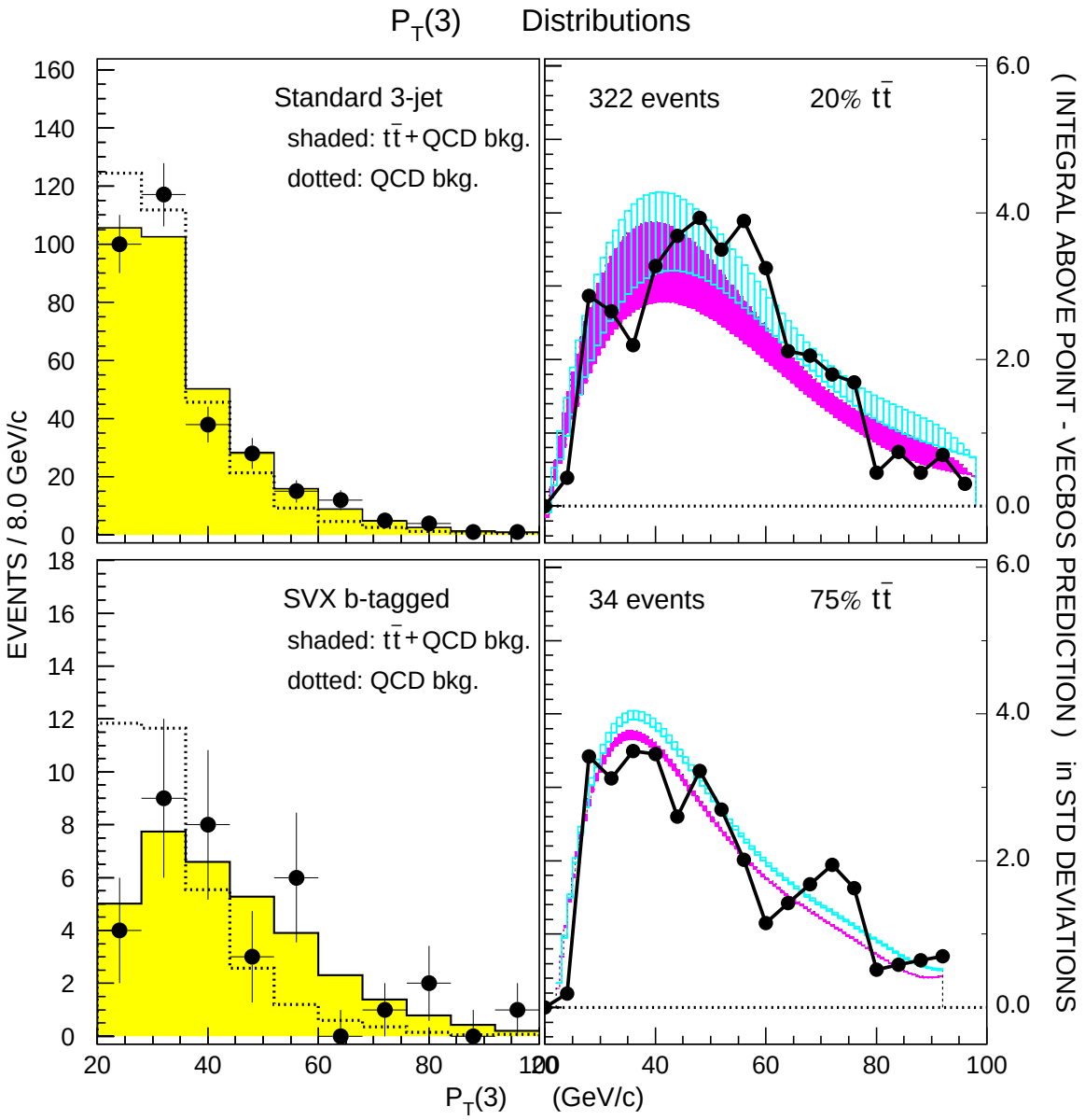

FIG. 13. Comparison of the data with Monte Carlo predictions for $P_T(3)$. Differential plots are on the left; the solid points with error bars are the data and the histograms are the Monte Carlo predictions normalized to the data. The integral significance plots are on the right; the data are the solid points. The shaded band is the prediction for the expected mixture of $t\bar{t}$ and QCD background for 175 GeV/c^2 top; the hatched band is the equivalent for 185 GeV/c^2 top. The width of the bands represent the uncertainty in the QCD background due to Q^2 scale variations. A data point one vertical unit from the shaded band corresponds to a one σ deviation.

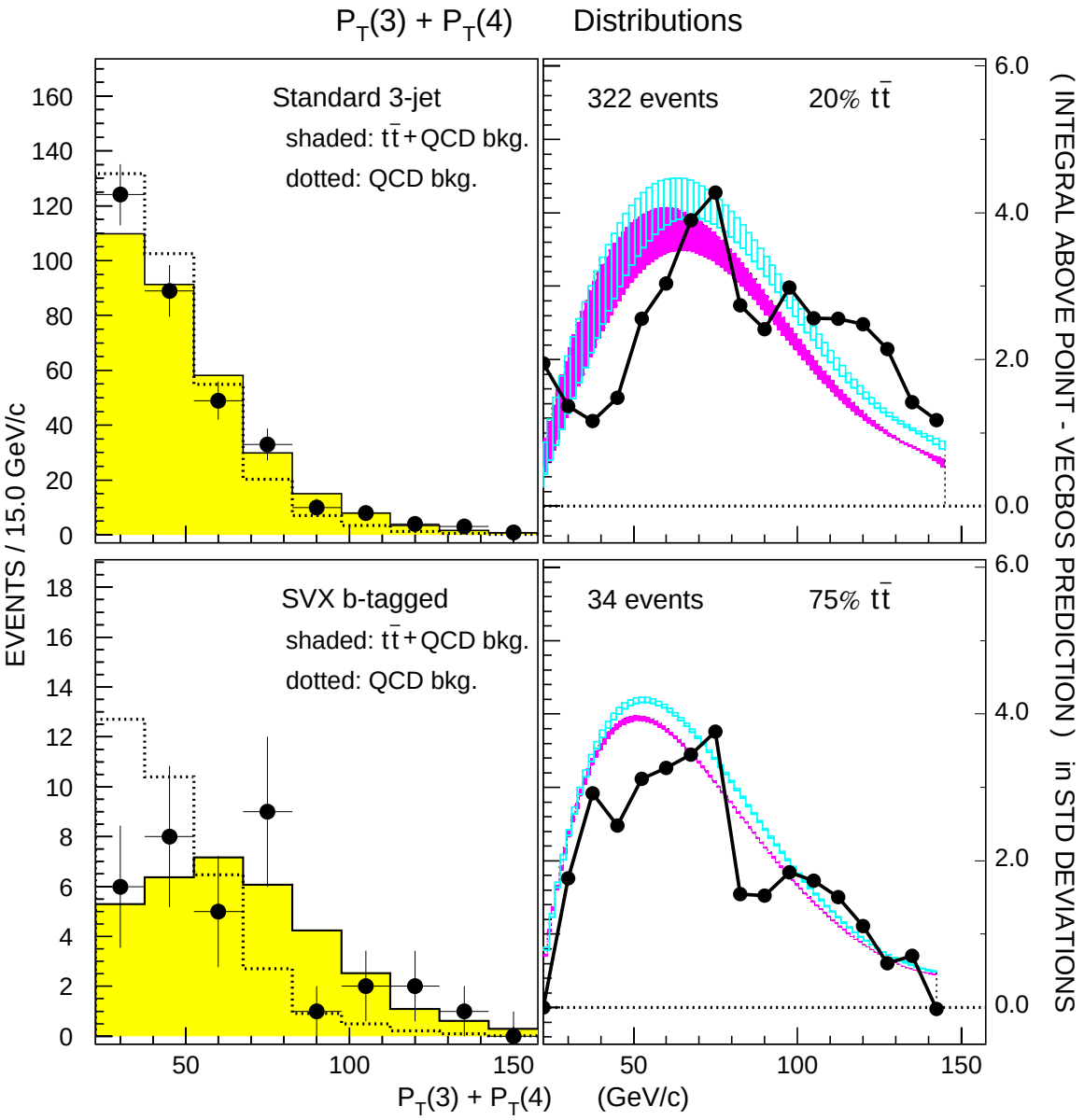

FIG. 14. Comparison of the data with Monte Carlo predictions for $P_T(3) + P_T(4)$. Differential plots are on the left; the solid points with error bars are the data and the histograms are the Monte Carlo predictions normalized to the data. The integral significance plots are on the right; the data are the solid points. The shaded band is the prediction for the expected mixture of $t\bar{t}$ and QCD background for 175 GeV/c^2 top; the hatched band is the equivalent for 185 GeV/c^2 top. The width of the bands represent the uncertainty in the QCD background due to Q^2 scale variations. A data point one vertical unit from the shaded band corresponds to a one σ deviation.

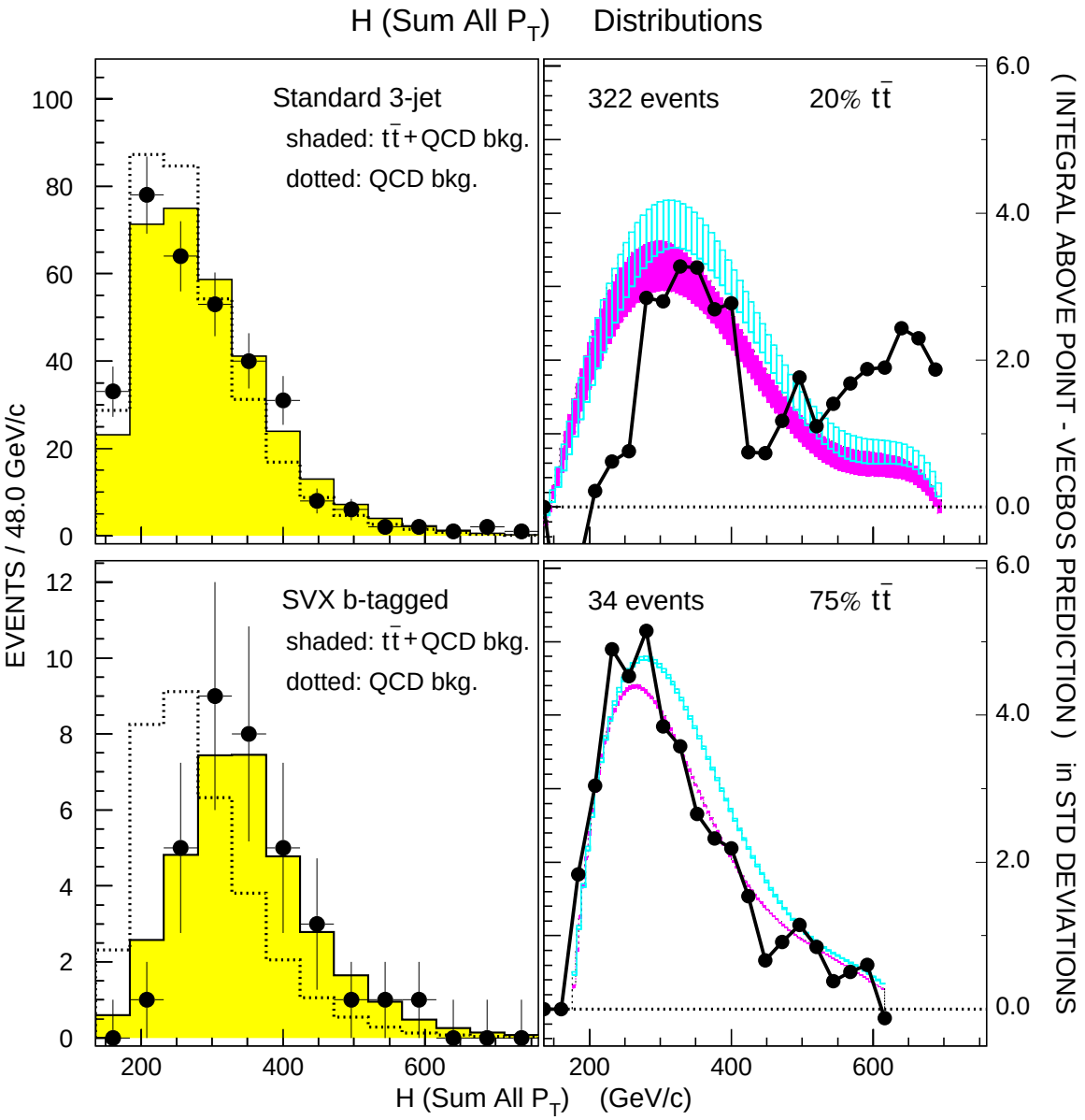

FIG. 15. Comparison of the data with Monte Carlo predictions for H. Differential plots are on the left; the solid points with error bars are the data and the histograms are the Monte Carlo predictions normalized to the data. The integral significance plots are on the right; the data are the solid points. The shaded band is the prediction for the expected mixture of $t\bar{t}$ and QCD background for 175 GeV/c^2 top; the hatched band is the equivalent for 185 GeV/c^2 top. The width of the bands represent the uncertainty in the QCD background due to Q^2 scale variations. A data point one vertical unit from the shaded band corresponds to a one σ deviation.

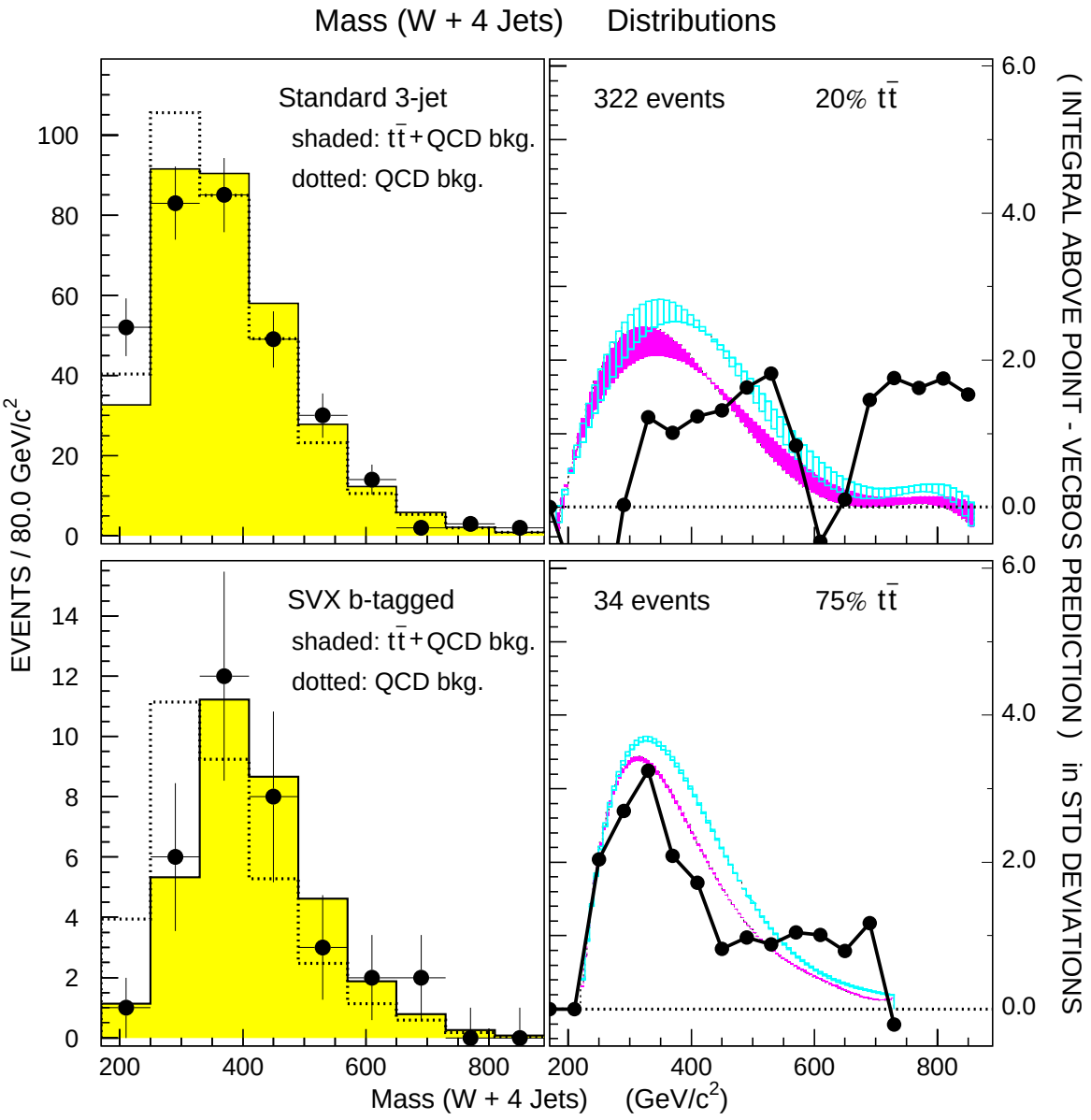

FIG. 16. Comparison of the data with Monte Carlo predictions for Mass(W + 4 Jets). Differential plots are on the left; the solid points with error bars are the data and the histograms are the Monte Carlo predictions normalized to the data. The integral significance plots are on the right; the data are the solid points. The shaded band is the prediction for the expected mixture of $t\bar{t}$ and QCD background for 175 GeV/c^2 top; the hatched band is the equivalent for 185 GeV/c^2 top. The width of the bands represent the uncertainty in the QCD background due to Q^2 scale variations. A data point one vertical unit from the shaded band corresponds to a one σ deviation.

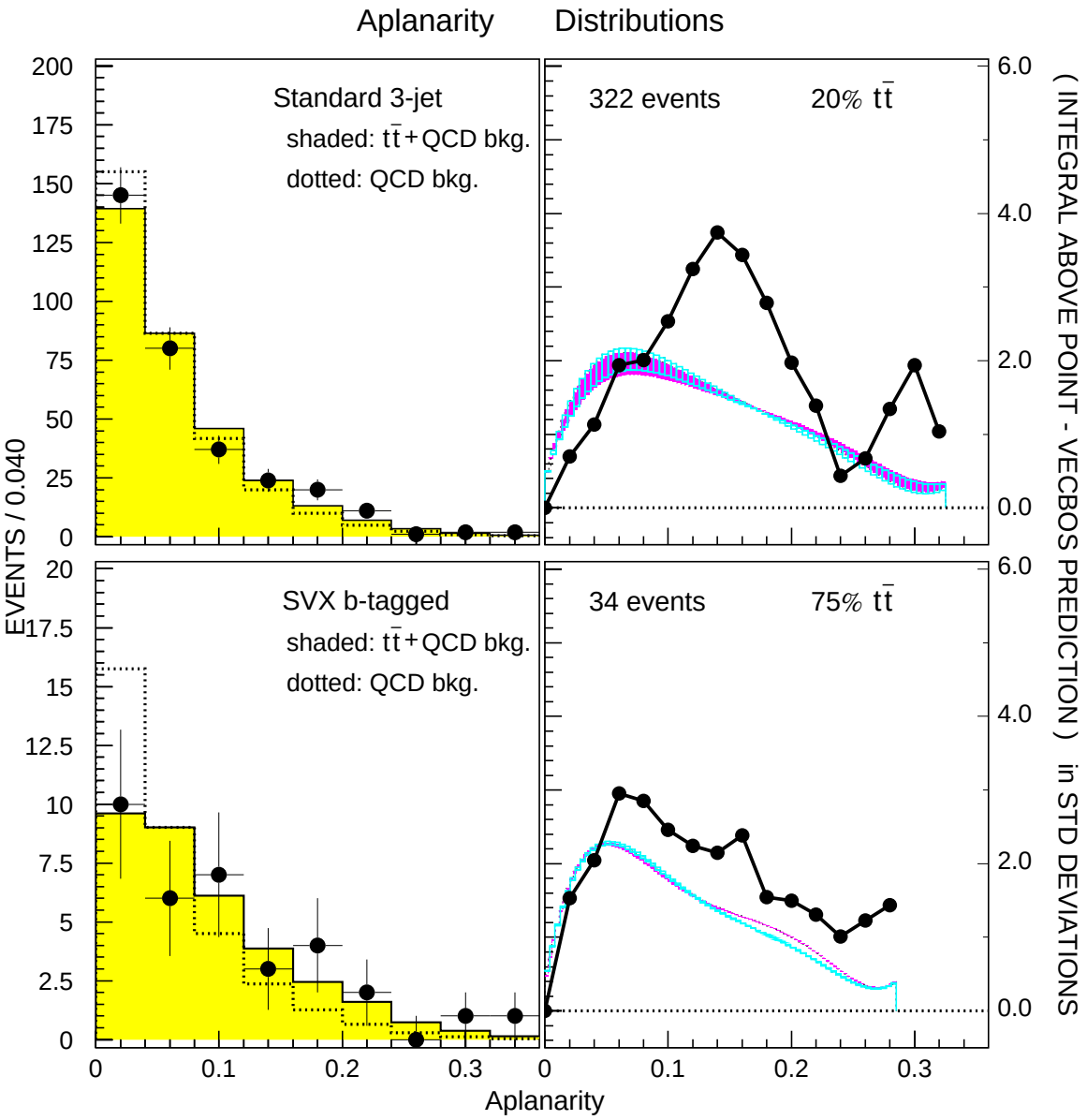

FIG. 17. Comparison of the data with Monte Carlo predictions for the aplanarity. Differential plots are on the left; the solid points with error bars are the data and the histograms are the Monte Carlo predictions normalized to the data. The integral significance plots are on the right; the data are the solid points. The shaded band is the prediction for the expected mixture of $t\bar{t}$ and QCD background for 175 GeV/c^2 top; the hatched band is the equivalent for 185 GeV/c^2 top. The width of the bands represent the uncertainty in the QCD background due to Q^2 scale variations. A data point one vertical unit from the shaded band corresponds to a one σ deviation.